

1 **Replies to: Anonymous Referee #3.** Interactive comment on “The ENSO signal in
2 atmospheric composition fields: emission driven vs. dynamically induced changes” by A.
3 Inness et al.

4 Received and published: 8 June 2015

5 *We thank Referee 3 for their useful comments about our paper. We have tried to address all*
6 *the suggestions and revised the manuscript accordingly. Our replies to their comments are*
7 *given below in blue and changes to the manuscript in bold and blue.*

8 General comments:

9 The manuscript presents results on the changes in atmospheric composition in the MACC
10 system resulting from the ENSO. Differences in ozone, CO and NO₂ concentrations between
11 composites of El-Nino and La-Nina years are used to evaluate the role of changes in emission
12 and dynamics on the atmospheric composition in the tropics. The first part of the paper
13 presents differences in chemical composition in the MACC system dataset over a 10 year
14 time period. The specific role of changes in emission or changes in dynamics is addressed in
15 a second part with the C-IFS model which is run during a El-Nino year and a weak La-Nina
16 year with different emission scenario. The authors conclude that changes in ozone over
17 Indonesia are associated with changes in photochemical production due to an increase in
18 biomass burning emission during El- Nino periods. Large scale ozone anomalies are found
19 over the Pacific due to changes in vertical transport. Anomalies in CO, NO₂ and AOD are
20 mostly found over the maritime continent and are related to changes in biomass burning
21 emission. I recommend the paper for publication after addressing the following comments.

22 Specific comments:

23 1) Last paragraph, page 13721: the authors claim that the MACC system can
24 successfully model the ENSO signal. Because there is no validation of the ENSO signal
25 against measurements, I cannot agree with this conclusion. Even though the MACC
26 system was compared to satellite products in Inness et al. (2013), we need to see
27 such validation for The ENSO signal, as it is estimated by subtracting El-Nino and La-
28 Nina time periods. Inness et al. (2013) discussed only monthly averaged biases
29 between MACC and satellite products. Bias and/or uncertainties specific to the ENSO
30 signal in the MACC system could exist. It is particularly important if subsequent
31 studies will deal with ocean-atmosphere interactions and ocean-atmosphere
32 response to ENSO. If the atmospheric response in terms of terrestrial emission and
33 dynamics is not well represented, how one can expect to have meaningful
34 conclusions on ocean-atmosphere response and impact on atmospheric
35 composition?

36 *We have changed that sentence to:*

1 *The results from this paper show that the MACC system is able to model changes in*
2 *atmospheric composition fields found under El Niño and La Niña conditions. After a*
3 *more thorough validation of the MACC atmospheric fields against observations, it*
4 *could be interesting to investigate the ocean-atmosphere response to ENSO induced*
5 *changes in atmospheric composition in a further study.*
6

7 The way atmospheric dynamics is treated in section 2 is not convincing. The
8 affirmations on the impact of dynamics on atmospheric composition in section 2 is
9 only discussed in general terms since not enough meteorological fields are
10 presented. Section 3 is much more convincing because it uses vertical velocity and
11 specific humidity. Vertical velocity and specific humidity should be used in the first
12 part of the analysis as well.

13 *We have produced composites of vertical velocity and specific humidity at 500 hPa*
14 *from the MACC reanalysis and added the El Nino minus La Nina difference plots as*
15 *Figure 2 to the paper (the numbers of the subsequent figures have been changed in*
16 *the revised manuscript, but we use the original numbers in our replies to the*
17 *reviewers further below). We have added in the text:*

18 ***Figure 2 shows that the increased precipitation over the Central Pacific and the***
19 ***reduced precipitation over the Maritime continent are collocated with increased***
20 ***ascent and increased descent at 500 hPa, respectively. At the same time, specific***
21 ***humidity at 500 hPa shows a positive anomaly in the area of increased ascent and***
22 ***precipitation over the Central Pacific and a negative anomaly over the Maritime***
23 ***continent.***
24

- 25 2) Changes in cloud cover during La-Nina and El-Nino years can also affect ozone
26 photochemical production. Maps of J(O1D) photolysis rate would provide additional
27 insight into section 2 and 3.

28 *Unfortunately, this is not available from the MACC reanalysis and would require a re-*
29 *run of the experiments in Section 3. In general, the impact of increased cloud cover*
30 *results in a reduction of JO1D below and increase of JO1D above the clouds, which is*
31 *often compensating the OH production. Anomalies of cloud cover at 500 hPa show a*
32 *similar signal to humidity (our new Figure 2) with decreased cloud cover over*
33 *Indonesia and increased cloud cover over the central Pacific. A detailed analysis of the*
34 *chemical budgets for this situation would make an interesting future study, but is*
35 *beyond the scope of the current paper. We have added a sentence about the cloud*
36 *cover in Section 2.2: **Cloud cover shows a similar signal to humidity, with a negative***
37 ***anomaly over the Maritime continent and a positive anomaly over the central***
38 ***Pacific (not shown).***
39

- 1 3) Why formaldehyde is not treated in the paper? Atmospheric composition should not
2 be limited to ozone, CO and NO₂.

3 *The reviewer is correct that formaldehyde (HCHO) is an interesting species as it points*
4 *at varying isoprene sources in the region, which may in turn affect O₃ production,*
5 *depending on availability of NO_x. Unfortunately, in current simulations HCHO is not*
6 *constrained in the MACC system by observations and biogenic emissions are applied*
7 *without inter-annual variability. Therefore we do not believe that HCHO is a suitable*
8 *tracer to analyse for this paper.*

- 9
10 4) How biomass burning is injected vertically in the model? Since the injection height
11 will be affected by fire intensity and atmospheric stability, one can expect a change in
12 injection height during El-Nino vs La-Nina. If a fixed injection height is used, it could
13 bias the CO and AOD fields at 500hPa.

14 *We have added in section 2.1 :*

15 *The emissions are injected at the surface and distributed over the boundary layer*
16 *by the model's convection and vertical diffusion scheme. Despite the distribution*
17 *being very efficient, this is a limitation of the current system that and will be*
18 *addressed in future versions. Experiments have been carried out with a new version*
19 *that uses injection heights based on the Plume Rise Model of Paugam et al. (2015).*
20 *They show a significant impact on BC AOD for single large fires; the impact at a*
21 *global scale is smaller: BC AOD is increased by around 5%. Most of the injections*
22 *heights calculated with the Plume Rise Model lie within the boundary layer and*
23 *only a small fraction of smoke (often from particularly intense, and well-studied*
24 *fires) is injected directly into the free troposphere. The largest smoke transport*
25 *from the boundary layer to the free troposphere occurs through larger-scale*
26 *meteorological processes. The lowering of the boundary layer height, when air is*
27 *advected from land to sea, and strong updrafts in frontal system have previously*
28 *been identified as efficient smoke transport mechanisms. Similarly, Veira et al.*
29 *(2015) has studied the sensitivity of AOD in a global climate model to different*
30 *injection height parameterisations and the above-mentioned plume rise model,*
31 *with the conclusion that a simple parameterisation reproduces the average larger-*
32 *scale distribution sufficiently well.*

33 *Extra reference: Paugam, R., Wooster, M., Atherton, J., Freitas, S. R., Schultz, M. G.,*
34 *and Kaiser, J. W.: Development and optimization of a wildfire plume rise model based*

1 *on remote sensing data inputs – Part 2, Atmos. Chem. Phys. Discuss., 15, 9815-9895,*
2 *doi:10.5194/acpd-15-9815-2015, 2015.*

3 *Veira, A., Kloster, S., Schutgens, N. A. J., and Kaiser, J. W.: Fire emission heights in the*
4 *climate system – Part 2: Impact on transport, black carbon concentrations and*
5 *radiation, Atmos. Chem. Phys., 15, 7173-7193, doi:10.5194/acp-15-7173-2015, 2015.*

- 6
7 5) How ocean emission of halogenated species, VOCs and deposition on ocean surface
8 is treated?

9 *We have added in Section 2.1: **The MACC models do not contain halogenated***
10 ***species, which would contribute to a small additional loss term to O3 and its***
11 ***precursors in the tropical marine boundary layer. Ocean emissions of volatile***
12 ***organic compounds (VOCs) originate from climatological data from POET.***
13 ***Deposition on ocean surface depends on the species solubility, which is negligible***
14 ***for O3 and CO, but not for some of the VOCs. All these aspects may contribute to***
15 ***overall biases in the model, but are not considered essential for the signals***
16 ***investigated here.***

- 17
18 6) section 2: Why the AOD anomaly reach the lower troposphere at 200E, but no such
19 anomaly is found in CO, NOx and ozone?

20
21 *We have added at the end of Section 2:*
22 ***In the lower troposphere there is a negative aerosol anomaly over the Central***
23 ***Pacific that is not seen in the other atmospheric composition fields. This anomaly is***
24 ***likely to be the result of the increased precipitation in this area during El Niño***
25 ***conditions (see Figure 1) which leads to increased wet deposition and removal of***
26 ***aerosols, while not removing the gas-phase species in the same way.***

27 Technical comments:

28 line 18, p13711: la nina ...

29 *Changed*

30 line 11, p13721: comparing simulations ...

31 *Changed*

32

1
2

3 **Replies to: Dr. Nassar (Referee).** Interactive comment on “The ENSO signal in atmospheric
4 composition fields: emission driven vs. dynamically induced changes” by A. Inness et al.

5 Received and published: 14 June 2015

6 *We thank Dr. Nassar for his useful comments about our paper. We have tried to address all*
7 *the suggestions and revised the manuscript accordingly. Our replies to their comments are*
8 *given below in blue and changes to the manuscript in bold and blue.*

9 Inness et al. use the Monitoring Atmospheric Composition and Climate (MACC) reanalysis to
10 investigate the effects of El Nino on atmospheric composition, specifically CO, ozone, NOx
11 and aerosol in the region of the Maritime continent. The manuscript was very well-written
12 and clearly presented, with minimal errors and high quality figures. The work described in
13 this manuscript builds off of many previous studies on the impact of El Nino on atmospheric
14 composition. While most previous studies focused on a single El Nino event relative to a
15 neutral or La Nina year, Inness et al. investigate October, November and December
16 composites from three El Ninos (2004, 2006, 2009) compared with composites from those
17 months during La Nina (2005, 2007, 2008, 2010) from their 10-year MACC reanalysis. This
18 reanalysis is at a far higher spatial resolution (80 km) than any known past global modeling
19 studies on this topic, so in this sense the study is an advance relative to earlier work,
20 however, the scientific investigation does not go as far as in some earlier work, which was a
21 bit of a disappointment. For example, the authors separate the El Nino impacts on
22 atmospheric composition into emissions and dynamics, and conclude that the ozone
23 enhancement is mostly dynamical, but according to their method, their dynamical
24 component must include the contribution from lightning NOx emissions, which is only briefly
25 mentioned without an attempt to quantify the lightning impact on ozone.

26 *Dr. Nassar is correct that our dynamical component includes the contribution from lightning*
27 *NOx on ozone, as this contribution is not isolated in our study. Alike, also the wet scavenging*
28 *is not separated from the dynamical component or the impact of cloudiness on photolysis*
29 *rates. It is fair to say that we basically mean meteorological (or atmospheric) factors when*
30 *we say „dynamics“. In this study we wanted to isolate the impact of the biomass burning*
31 *emissions. We argue that lightning NOx production is considered as an inseparable aspect of*
32 *the dynamical component in this study, as the flash rate density that is used to calculate NO*
33 *emissions from lightning is based on parameters of the convection scheme and is calculated*
34 *using convective precipitation as input parameter. This parameter is affected by changes in*
35 *the dynamics and not the fire emissions. In a future study it could be of interest to assess the*
36 *chemical budgets in more detail but that is beyond the scope of the current paper.*

1 In general, a more quantitative evaluation of the MACC reanalysis would have been
2 desirable. For example, the authors state in their conclusion (p 13721) that the results of the
3 paper show that “the MACC system is able to successfully model the ENSO signal in
4 atmospheric composition fields, and could therefore be used in further studies to investigate
5 the ocean-atmosphere response to ENSO induced changes in atmospheric composition.”
6 However, they do not demonstrate that the ozone, NO_x and CO enhancements in the
7 reanalysis during an El Nino do indeed match observations. Inness et al. 2013 is cited, but
8 this is just a general comparison paper and does not demonstrate the agreement specifically
9 in this region during El Nino. Perhaps this is because observations have been assimilated, so
10 the fields are assumed to match observations, which may generally be the case, but reader
11 has no knowledge of the degree of agreement with observations without it being
12 demonstrated here. This contrasts with for example, Nassar et al. (2009) in which GEOS-
13 Chem CO, ozone and water vapour composition fields generally agree with satellite
14 observations, however, attempts were made to explain remaining differences between the
15 model and observations by investigating issues like: the magnitude and timing of CO
16 emission, possibly related to the model and biomass burning inventory’s neglect of peat
17 smouldering; the impact of enhanced lightning NO_x and soil NO_x on the ozone
18 enhancement; or the impact of convective transport on CO, ozone and water vapour. Since
19 Inness et al. does not quantitatively confirm the magnitude and timing of the anomalies in
20 the reanalysis with independent observations, one can only make conclusions regarding the
21 relative contributions of emissions and dynamics in the MACC system, but cannot reliably
22 extend such conclusions to the real earth system.

23 In summary, while this paper in its current form (with minor corrections) can be considered
24 a reasonable and a useful introductory analysis of MACC during El Nino, a quantitative
25 verification of the MACC El Nino composition fields in this region using observations, AND
26 hypotheses to explain any differences, would make this a stronger paper, perhaps enhancing
27 our scientific understanding of the topic.

28 *A detailed quantitative verification of the MACC El Nino composition fields is beyond the*
29 *scope of this paper, but we agree with Dr. Nassar that it would be worth while to do this in a*
30 *follow up study. A basic validation of the fields was done in Inness et al (2013), Inness et al.*
31 *(2015) and Flemming et al. (2015) and more detailed validation is constantly carried out by*
32 *the MACC validation team whose validation reports are available from*
33 *<http://www.copernicus-atmosphere.eu/>. We already mention the reanalysis validation*
34 *reports in Section 2.1. We have added a reference to Inness et al. (2015) and have also added*
35 *in Section 3.1: **A basic initial validation of CIFS-fields can be found in Flemming et al. (2015)***
36 ***and Inness et al. (2015) and more detailed validation of C-IFS can be found in the validation***
37 ***reports available from <http://www.copernicus-atmosphere.eu/>.***

38 **Specific points**

1 p 13706, line 12: “nitrogen oxide” should be “nitrogen oxides”
2 *Corrected.*

3 p 13714, line 14: “EL” should be “El”
4 *Corrected.*

5 p 13714, line 23: “upper the troposphere” should be “upper troposphere”
6 *Corrected.*

7 p 13715, line 4: the longitude for the anomaly in Figure 9 that they are referring to would be
8 helpful to provide. They mention an anomaly over Africa, which I’d expect at 30 E, whereas a
9 positive anomaly appears over 300E or South America.

10 *Sorry, this was wrong in the text. We have changed it to: **Now a small positive anomaly is***
11 ***found over South America.***

12 p 13716, line 15: “lighning” should be “lightning”
13 *Corrected.*

14 p 13718, line 15: “surrunding” should be “surrounding”
15 *Corrected.*

16 p 13721, line 11: “Comapring” should be “Comparing”
17 *Corrected.*

18 p 13721, line 17: “affected” should be “affected”
19 *Corrected.*

20 Figure 10. A more detailed interpretation of the NO_x anomalies is desirable.
21 *We have added in the discussion of Figure 10:*

22 ***The positive NO_x anomalies around 100°E in October and November are collocated with***
23 ***high O₃ values in the lower troposphere (seen in Figure 8) pointing to enhanced O₃***
24 ***production due to enhanced NO_x concentrations from biomass burning. In December,***
25 ***when NO_x does not show such a positive anomaly any more, O₃ concentrations in the***
26 ***lower troposphere are lower and the maximum of the O₃ anomaly is located above***
27 ***700hPa.***

1 Figure 15. The authors fail to comment on the fact that in October, the peak in specific
2 humidity is south of ozone enhancement. Nassar et al. (2009) showed that the equa- torial
3 component of the October ozone anomaly was related to fire emissions, with the southern
4 component of the ozone anomaly due to other factors.

5 *We have added in the paper:*

6 ***In October the peak in specific humidity is located south of the ozone enhancement. This***
7 ***agrees with Nassar et al. (2009) who showed that the equatorial component of the***
8 ***October ozone anomaly was related to fire emissions, while the southern component of the***
9 ***ozone anomaly was due to other factors.***

10 Furthermore, that fact that the elevated humidity over southern Africa corresponds to
11 decreased ozone, but a similar feature over in the region of Saudi Arabia and Iran does not,
12 warrants some comment.

13 *We have added in the paper:*

14 ***It should be noted that the positive specific humidity anomalies over the Arabian peninsula***
15 ***and over Australia in October do not correspond to decreased ozone values, while the ones***
16 ***over southern Africa, South America and the Central Pacific do. The reason for this is that***
17 ***relative anomalies are shown and that the absolute humidity values over the Arabian***
18 ***peninsula and Australia are much lower than in the other areas, so that the absolute***
19 ***humidity changes between 2006 and 2005 are actually relatively small. This all suggests***
20 ***that the correlation of O₃ to specific humidity is strongest in tropical regions with large***
21 ***variability in water vapour, combined with low NO_x conditions.***

22 Figure 17. It would have been useful to show a larger longitude range for the map here
23 (especially westward) since in panel b, for example, major features are cut off at the map
24 boundaries.

25 *We have increased the area to the west so that it now extends from 40E to 130E.*

26

1
2

3 **Replies to M.-Y. Lin:** Interactive comment on “The ENSO signal in atmospheric composition
4 fields: emission driven vs. dynamically induced changes” by A. Inness et al.

5 Received and published: 22 June 2015

6 This comment is posted by Meiyun Lin (Princeton University). The role of emission driven
7 versus dynamically induced changes in atmospheric composition in association with ENSO is
8 a very interesting topic. The following two publications particularly addressed this question,
9 and thus are highly relevant to many discussions in your paper. Meiyun Lin, L.W. Horowitz, S.
10 J. Oltmans, A. M. Fiore, Songmiao Fan (2014): Tropospheric ozone trends at Manna Loa
11 Observatory tied to decadal climate variability, Nature Geoscience, 7, 136-143,
12 doi:10.1038/NGEO2066.

13 Meiyun Lin, A.M. Fiore, L.W. Horowitz, A.O.Langford, S. J. Oltmans, D. Tarasick, H.E. Reider
14 (2015): Climate variability modulates western US ozone air quality in spring via deep
15 stratospheric intrusions, Nature Communications, 6, 7105, doi:10.1038/ncomms8105

16 Despite large El Nino enhancements to wildfire activity in equatorial Asia, the model
17 sensitivity experiments in Lin et al (2014, Nature Geosci) indicate that wildfire emissions are
18 not the main driver of ENSO-related ozone variability observed at Mauna Loa, Hawaii (Figure
19 3). The dynamically induced eastward extension and equatorward shift of the subtropical jet
20 stream during El Nino plays a key role on observed interannual variability of springtime
21 lower tropospheric ozone at Mauna Loa. These shifts enhance long range transport of Asian
22 ozone and CO pollution towards the eastern North Pacific in winter and spring during El
23 Nino.

24 Lin et al (2015, Nature Communications) demonstrated a connection between springtime
25 western US ozone air quality and jet characteristics associated with strong La Nina winters.
26 They showed more frequent late spring deep stratospheric ozone intrusions when the polar
27 jet stream meanders southward over the western United States as occurs following strong
28 La Nina winters. Their finding again reflects the dynamically driven changes in atmospheric
29 composition in association with ENSOT.

30 *Thanks for pointing out these extra references. We have included them in Section 3.2 of the*
31 *paper: **The importance of the dynamically driven ozone changes was also highlighted by***
32 ***Lin et al. (2014 and 2015). Despite large El Nino enhancements to wildfire activity in***
33 ***equatorial Asia, the model sensitivity experiments in Lin et al. (2014) indicated that***
34 ***wildfire emissions are not the main driver of ENSO-related ozone variability observed at***
35 ***Mauna Loa, Hawaii. The dynamically induced eastward extension and equatorward shift***
36 ***of the subtropical jet stream during El Nino plays a key role on observed interannual***

1 *variability of springtime lower tropospheric ozone at Mauna Loa. These shifts enhance*
2 *long range transport of Asian ozone and CO pollution towards the eastern North Pacific in*
3 *winter and spring during El Nino. Lin et al. (2015) demonstrated a connection between*
4 *springtime western US ozone air quality and jet characteristics associated with strong La*
5 *Nina winters. They showed more frequent late spring deep stratospheric ozone intrusions*
6 *when the polar jet stream meanders southward over the western United States as occurs*
7 *following strong La Nina winters.*

8

1

2 **The ENSO signal in atmospheric composition fields:** 3 **Emission driven versus dynamically induced changes**

4

5 **A. Inness¹, A. Benedetti¹, J. Flemming¹, V. Huijnen², J.W. Kaiser³, M.**
6 **Parrington¹ and S. Remy⁴**

7

8 [1] {ECMWF, Reading, UK}

9 [2] {Royal Netherlands Meteorological Institute, De Bilt, The Netherlands}

10 [3] {Max-Planck-Institute for Chemistry, Mainz, Germany}

11 [4] {Laboratoire de Météorologie Dynamique, Paris, France}

12 Correspondence to: A. Inness (a.inness@ecmwf.int)

13

14 **Abstract**

15 The El Niño Southern Oscillation (ENSO) does not only affect meteorological fields but also
16 has a large impact on atmospheric composition. Atmospheric composition fields from the
17 Monitoring Atmospheric Composition and Climate (MACC) reanalysis are used to identify the
18 ENSO signal in tropospheric ozone, carbon monoxide, nitrogen oxide and smoke aerosols,
19 concentrating on the months October to December. During El Niño years all these fields have
20 increased concentrations over Maritime South East Asia in October. The MACC Composition
21 Integrated Forecasting System (C-IFS) model is used to quantify the relative magnitude of
22 dynamically induced and emission driven changes in the atmospheric composition fields. While
23 changes in tropospheric ozone are a combination of dynamically induced and emission driven
24 changes, the changes in carbon monoxide, nitrogen ~~oxide~~oxides and smoke aerosols are almost
25 entirely emission driven in the MACC model. The ozone changes continue into December, i.e.
26 after the end of the Indonesian fire season while changes in the other fields are confined to the
27 fire season.

28

1

2 **1 Introduction**

3 The El Niño Southern Oscillation (ENSO) is the dominant mode of variability in the Tropics
4 (e.g. Allan et al. 1996). It does not only affect meteorological fields but has a large impact on
5 atmospheric composition too, for example on ozone (O₃), carbon monoxide (CO), nitrogen
6 oxides (NO_x) and aerosols (e.g. Logan et al. 2008; Ziemke and Chandra, 2003, Chandra et al.,
7 2002; Wang et al., 2004). As the result of an eastwards shift of the warm sea surface
8 temperatures (SST) and the large scale Walker circulation anomaly in the tropical Pacific during
9 El Niño years, downward motion is increased and convection and precipitation are reduced over
10 the Western Pacific and the Maritime Continent. During La Niña conditions the opposite
11 dynamical effects occur. Fire emissions over Indonesia show a large interannual variability
12 (IAV), with largest emissions during El Niño years (e.g. van der Werf et al., 2006, Kaiser et al.,
13 2012), when drought conditions and anthropogenic biomass burning lead to big wild fires
14 (Duncan et al., 2003; Lyon et al., 2004; Page et al., 2002) that emit large amounts of trace gases
15 and aerosols. During El Niño years tropospheric O₃ columns (TCO₃) are decreased over the
16 Central and Eastern Pacific and increased over the Western Pacific and Indonesia, while CO
17 concentrations and aerosols from biomass burning increase over Indonesia. Specific humidity
18 changes in the upper troposphere are anti-correlated with the changes in TCO₃ (e.g. Chandra
19 et al., 2007).

20 These atmospheric composition changes have been found in observations (Chandra et al., 1998;
21 Ziemke and Chandra 1999; Fujiwara et al., 1999; Chandra et al., 2007; Logan et al., 2008) and
22 were confirmed by modelling studies (Hauglustaine et al., 1999; Sudo and Takashashi, 2001;
23 Chandra et al., 2002; Doherty et al., 2006; Chandra et al., 2009; Nassar et al., 2009) which also
24 tried to quantify the relative importance of the dynamically induced and the emission driven
25 atmospheric composition changes. The reasons for the TCO₃ increase over the Western Pacific
26 and Indonesia during El Niño years are (i) changes in the vertical transport that lead to enhanced
27 downward transport of O₃ rich air from the upper troposphere (and perhaps stratosphere) to the
28 middle and lower troposphere, and reduced transport of O₃ poor air from the lower troposphere
29 into the upper troposphere; (ii) a longer chemical lifetime of O₃ because of reduced humidity
30 which affects the concentrations of the hydroxyl radical (OH) and hence the photochemical loss
31 of tropospheric O₃; and (iii) enhanced photochemical production of O₃ in the lower troposphere

1 because of increased concentrations of O₃ precursors from biomass burning, such as NO_x, CO
2 or Hydrocarbons. We refer to (i) and (ii) as ‘dynamically induced changes’ and to (iii) as
3 ‘emission driven changes’ throughout this paper.

4 For El Niño events with large fires over Indonesia, such as in 1997 and 2006, the TCO₃ changes
5 due to dynamics and due to increased emissions can be of similar magnitude (Sudo and
6 Takahashi, 2001; Chandra et al., 2002; Chandra et al., 2009), while for weaker events, such as
7 the 2004 El Niño, the dynamical impact dominates (Chandra et al., 2007).

8 The changes in CO are mainly emissions driven (Logan et al., 2008; Chandra et al., 2009;
9 Voulgarakis et al., 2010) and of smaller horizontal scale than the O₃ anomalies, but dynamical
10 interactions due to changes in water vapour (H₂O) and hence OH can also play a role. CO is
11 increased over the Western Pacific and the Maritime Continent during El Niño because of
12 increased emissions from fires and the increased chemical lifetime due to reduced OH. The CO
13 anomaly over Indonesia is usually gone by December (Logan et al., 2008; Chandra et al., 2009),
14 after the end of the biomass burning season, while the O₃ anomaly continues.

15 Large Indonesian wildfires can affect the air quality over South East Asia. Aouizerats et al.
16 (2015) investigated how the transport of biomass burning emissions from Sumatra affected the
17 air quality in Singapore. They found that 21% of the PM₁₀ loading in Singapore during July to
18 October 2006 was due to Sumatran fires, and that Sumatran fires were responsible for about
19 half of the days with PM₁₀ concentrations greater than 50 µgm⁻³ while the other half was due to
20 local anthropogenic pollution and contributions from smaller fires. The impact of fire emissions
21 on atmospheric aerosol concentrations is of particular interest because of the potential
22 feedbacks of fire-induced aerosols on climate. Several studies have looked at the correlations
23 between ENSO and aerosols or atmospheric haze produced by the Indonesian fires. Wang et al.
24 (2004) used visibility data over Sumatra as an indicator of biomass burning and found that haze
25 events were strongly correlated with El Niño during the 1973 to 2003 period. Tosca et al. (2010)
26 used satellite data and modelling studies and found that the aerosol optical depth (AOD) over
27 Indonesia had a large IAV that was driven by wild fires during periods of El Niño induced
28 droughts. Their modelling study showed that the fire-emitted aerosols could initiate a positive
29 feedback loop. The aerosols acted to intensify drought over the biomass burning regions. The
30 aerosols also reduced land and sea surface temperatures, and hence suppressed convection and
31 precipitation in the area. Podgorny et al. (2003) looked at the feedback between El Niño and

1 the Indonesian biomass burning of 1997 and also found that the haze from the fires reduced the
2 solar radiation absorbed by the equatorial Indian Ocean and increased the solar heating of the
3 atmosphere, thus raising the possibility of dynamical feedbacks of the smoke forcing on ENSO.
4 Chung and Ramanathan (2003) carried out modelling studies to assess the remote impact of
5 changes in the South Asian haze and found that fluctuations in the absorbing aerosol forcing
6 could affect the interannual climate variability in the Tropics (and Extratropics). It could
7 remotely suppress convection in the equatorial western Pacific and lead to an ocean-atmosphere
8 response that was very similar to El Niño like warming.

9 As part on the EU FP7 funded Monitoring Atmospheric Composition and Climate (MACC)
10 project (www.copernicus-atmosphere.eu) a 10-year reanalysis of atmospheric composition
11 (Inness et al. 2013) was constructed. This reanalysis provides fields of chemically active gases,
12 for example CO, O₃, and NO_x, as well as aerosols globally for both the troposphere and the
13 stratosphere for the years 2003 to 2012. It gives us the unprecedented possibility to assess the
14 impact of ENSO on atmospheric composition using an observationally constrained, continuous,
15 3-dimensional atmospheric composition dataset with a resolution of about 80 km, which is
16 greater than the resolutions used in most previous modelling studies. In this paper we show that
17 the MACC reanalysis shows the ENSO induced anomalies in O₃, CO, NO_x and aerosols
18 described in earlier studies. We then use MACC's Composition Integrated Forecasting System
19 (C-IFS) model (Flemming et al. 2015) to quantify the relative impact of the dynamics and the
20 biomass burning emissions on the ENSO signal in the O₃, CO, NO_x and smoke aerosol fields.

21 This paper is structured in the following way. Section 2 describes the MACC reanalysis and the
22 ENSO signal seen in MACC O₃, CO, NO_x and smoke aerosol fields. Section 3 describes the
23 additional C-IFS model runs that were carried out to quantify the relative impact of the
24 dynamics and biomass burning emission on the ENSO signal in the atmospheric composition
25 fields and their results, and Section 4 presents conclusions and outlook.

26

27 **2 ENSO signal in the MACC reanalysis**

28 **2.1 The MACC reanalysis**

29 The MACC data assimilation system provides analyses and forecasts of atmospheric
30 composition and was used to produce a reanalysis of atmospheric composition covering the

1 years 2003 to 2012, as described in Inness et al. (2013). O₃ retrievals from several instruments
2 (including the Ozone Monitoring Instrument (OMI), SCanning Imaging Absorption
3 spectroMeter for Atmospheric CHartographY (SCIAMACHY), Solar Backscatter Ultra-Violet
4 (SBUV/2), Microwave Limb Sounder (MLS)), CO retrievals from Measurements of Pollution
5 in the Troposphere (MOPITT) and the Infrared Atmospheric Sounding Interferometer (IASI),
6 tropospheric NO₂ columns from SCIAMACHY, and AOD from the Moderate Resolution
7 Imaging Sctroradiometer (MODIS) were assimilated to constrain the atmospheric
8 compostions fields. For more information about the assimilated datasets and the quality of the
9 O₃, CO, and NO_x fields produced by the analysis see Inness et al. (2013). The aerosol analysis
10 in the MACC reanalysis is similar to that described in Benedetti et al. (2009) and Morcrette et
11 al. (2011) and is based on 4-dimensional variational assimilation of AOD observations at 550
12 nm from the MODIS sensors, including a global adaptive bias correction. Comparisons of
13 multiyear averages of AOD over the period 2003–2010 from the MACC reanalysis and from
14 the Multi-angle Imaging SpectroRadiometer (MISR) sensors onboard the Terra satellite
15 indicate good qualitative agreement (not shown).

16 The anthropogenic emissions for the reactive gases for the MACC reanalysis were taken from
17 the MACCity inventory (Granier et al., 2011) which accounts for projected trends in the
18 emissions. For the aerosol fields they came from the EDGAR database (Dentener et al., 2006).
19 Monthly biomass burning emission for the years 2003 to 2008 from the GFED3.0 inventory
20 (van der Werf et al., 2010) were scaled to daily resolution using MODIS active fire
21 observations. From 2009 to 2012 daily biomass burning emissions from MACC's GFAS,
22 Version 1.0 (Kaiser et al. 2012) were used. One advantage of the MACC reanalysis is that it
23 used daily fire emission, in contrast to several other studies that used monthly averages.
24 Biogenic emissions used in the MACC reanalysis were for 2003. They came from a recent
25 update (Barkley, 2010) of the Model of Emissions of Gases and Aerosols from Nature version
26 2 (MEGAN2; Guenther et al. 2006, <http://acd.ucar.edu/~guenther/MEGAN/MEGAN.htm>) and
27 were used as monthly surface flux fields without interannual variation.

28 The emissions are injected at the surface and distributed over the boundary layer by the model's
29 convection and vertical diffusion scheme. Despite the distribution being very efficient, this is a
30 limitation of the current system that will be addressed in future versions. Experiments have
31 been carried out with a new version that uses injection heights based on the Plume Rise Model
32 of Paugam et al. (2015). They show a significant impact on BC AOD for single large fires; the

1 impact at a global scale is smaller: BC AOD is increased by around 5%. Most of the injection
2 heights calculated with the Plume Rise Model lie within the boundary layer and only a small
3 fraction of smoke (often from particularly intense and well-studied fires) is injected directly
4 into the free troposphere. The largest smoke transport from the boundary layer to the free
5 troposphere occurs through larger-scale meteorological processes. The lowering of the
6 boundary layer height, when air is advected from land to sea, and strong updrafts in frontal
7 systems have previously been identified as efficient smoke transport mechanisms. Similarly,
8 Veira et al. (2015) has studied the sensitivity of AOD in a global climate model to different
9 injection height parameterisations and the above-mentioned plume rise model, with the
10 conclusion that a simple parameterisation reproduces the average larger-scale distribution
11 sufficiently well.

12 The MACC models do not contain halogenated species, which would contribute to a small
13 additional loss term to O₃ and CO. Ocean emissions of volatile organic compounds (VOCs)
14 originate from climatological data from POET. Deposition on ocean surface depends on the
15 species solubility, which is negligible for O₃ and CO, but not for some of the VOCs. All these
16 aspects may contribute to overall biases in the model, but are not considered essential for the
17 signals investigated here.

18 Initial validation results from the MACC reanalysis are shown in Inness et al. (2013) and
19 Morcrette et al. (2011) and more detailed validation can be found in the MACC reanalysis
20 validation reports available from
21 http://atmosphere.copernicus.eu/services/aqac/global_verification/validation_reports/ .

22 **2.2 ENSO anomalies**

23 The MACC reanalysis was used to construct monthly composites of O₃, CO, NO_x fields at 500
24 hPa and of the smoke AOD, i.e. the sum of black carbon (BC) and organic matter (OM) AOD,
25 at 550 nm for El Niño and La Niña years for the months October, November and December.
26 The El Niño composite was constructed from the years 2004, 2006, 2009, the La Niña
27 composite from the years 2005, 2007, 2008, 2010, and 2011. Weak El Niño and La Niña years
28 were included in the composite calculation to increase the sample size. A recent timeseries of
29 the Multivariate ENSO index which was used to define the years used in our El Niño and La
30 Niña composites can be found on <http://www.esrl.noaa.gov/psd/enso/mei/index.html>.
31 Composites of vertical velocity and specific humidity at 500 hPa were also calculated from the

1 MACC reanalysis. SST and precipitation composite fields, that were not available from the
2 MACC reanalysis, were constructed for the same years from the ERA Interim reanalysis (Dee
3 et al. 2011), and biomass burning composites were calculated from the GFAS v1.0 data set. The
4 composites were then used to calculate anomalies for the various fields by taking the
5 difference between the El Niño and La Niña composites for the months October, November
6 and December.

7 Figure 1 shows the warm SST anomaly over the Central Pacific associated with El Niño
8 conditions and the resulting precipitation changes for October, November and December from
9 ERA Interim. Precipitation is increased over the central Pacific and reduced over the Western
10 Pacific, Maritime Continent, northern Australia and part of the Indian Ocean. Figure 2 shows
11 that the increased precipitation over the Central Pacific and the reduced precipitation over the
12 Maritime continent are collocated with increased ascent and increased descent at 500 hPa,
13 respectively. At the same time, specific humidity at 500 hPa shows a positive anomaly in the
14 area of increased ascent and precipitation over the Central Pacific and a negative anomaly over
15 the Maritime continent. Cloud cover shows a similar signal to humidity, with a negative
16 anomaly over the Maritime continent and a positive anomaly over the central Pacific (not
17 shown).

18 The increased biomass burning emissions related to the lack of rainfall over Indonesia and
19 Northern Australia can be seen in the FRP anomalies shown in Figure 23. Increased fire activity
20 can be seen over Indonesia in October and November, but has stopped by December after the
21 end of the fire season, while a weaker biomass burning anomaly continues in Northern Australia
22 into December. Over Brazil decreased fire activity can be seen in October.

23 Figure 34 shows the IAV of the biomass burning emissions for CO from GFAS v1.0 for the 10
24 years covered by the MACC reanalysis for the area around Indonesia (10°N and 10°S, 90°E and
25 130°E) and illustrates that the emissions are higher during the El Niño years 2004, 2006, 2009
26 than at other times. The largest values are seen for 2006. Table 1 shows the average CO, NO_x
27 and fire aerosol emissions from GFAS v1.0 during October, November, December for the El
28 Niño years and La Niña years. The average CO emissions during El Niño years during October,
29 November, and December are a factor of about 9, 12, and 2 larger, respectively, than during La
30 Niña years. For NO_x fire emissions the factors are 6, 7, 2 and for smoke aerosols 8, 10, 2,
31 respectively. The values in Table 1 are slightly smaller than the values in Chandra et al. (2009)

1 who list CO fire emissions over Indonesia as 44.2 Tg/month, 6.3 Tg/month and 0.2 Tg/months
2 and NO₂ fire emissions of 0.76, 0.11, and 0.0 for October, November, and December 2006,
3 respectively.

4 Figures 45 to 78 illustrate the impact that the dynamical and emission related changes have on
5 the atmospheric composition fields, by showing the anomalies calculated from the MACC
6 reanalysis at 500 hPa for O₃, CO, NO_x, and smoke AOD, respectively. O₃ shows positive
7 anomalies over the Western Pacific, Indonesia, Northern Australia and the Eastern Indian
8 Ocean, and negative anomalies over the Central and Eastern Pacific (Figure 45). These
9 anomalies are quite large scale and continue into December after the end of the biomass burning
10 anomaly over Indonesia. The O₃ anomalies agree well with those described in other studies
11 based on MLS and Total Ozone Mapping Spectrometer (TOMS) data (Chandra et al. 2009) as
12 well as Tropospheric Emission Spectrometer (TES) data (Logan et al. 2008). The negative O₃
13 anomaly over Africa and the western Indian Ocean in December was also noted by Nassar et
14 al. (2009) in TES data and modelling studies with the Goddard Earth Observing System 3-D
15 chemical transport model (GEOS-Chem), and we also note a negative O₃ anomaly over Brazil
16 in October. The O₃ anomalies are a combination of biomass burning changes and
17 meteorological changes as a consequence of changes in SSTs and the resulting eastward shift
18 of the Walker circulation (Sudo and Takahashi 2001; Chandra et al. 2002; Chandra et al. 2009).
19 The O₃ decrease over the Central and East Pacific is due to enhanced upward transport of O₃
20 poor air from the boundary layer into the middle and upper troposphere, and a shorter O₃
21 lifetime and larger photochemical loss due to increased H₂O (and hence OH) concentrations.

22 During October and November both dynamical and emission driven effects contribute, and
23 modelling studies (e.g. Sudo and Takahashi 2001; Chandra et al. 2002; Chandra et al. 2009)
24 have shown that emissions and dynamical changes can contribute equally for El Niño years
25 with strong biomass burning. The O₃ changes in December are due to the dynamical changes
26 after the end of the fire season over Indonesia. This agrees with what was seen by Logan et al.
27 (2008), Chandra et al. (2009) and Nassar et al (2009).

28 Figure 56 shows the CO anomalies at 500 hPa calculated from the MACC reanalysis. These
29 anomalies are more confined to the areas of the biomass burning anomalies (see Figure 23) than
30 the O₃ anomalies (Figure 45). The strongest positive anomaly is found over the Maritime
31 Continent during October and is linked to increased emissions from enhanced biomass burning

1 under drought conditions. A negative CO anomaly extends from South America over the
2 Southern Atlantic to Africa in October and is related to lower fire emissions over Brazil. Similar
3 anomalies were described by Logan et al. (2008), Nassar et al. (2009) and Chandra et al. (2009).
4 The CO anomalies during November are weaker than the October ones, and by December the
5 anomalies have all but disappeared. This confirms that the CO anomalies are mainly emission
6 driven and are not affected much by the dynamical changes that cause the O₃ anomalies after
7 the end of the biomass burning season in December.

8 The NO_x anomalies (Figure 67) clearly show the impact of the increased emissions from
9 biomass burning over Indonesia during October and November, but also seem to indicate some
10 large scale response. For example, the negative anomaly over the Eastern Pacific is colocated
11 with the negative O₃ anomaly here (Figure 45) and could indicate enhanced upward transport
12 of NO_x poor air to these levels. Also the negative NO_x anomaly over the Pacific in December
13 is again co-located with a (larger) negative O₃ anomaly.

14 Figure 78 shows the anomaly of smoke AOD at 550 nm calculated from the MACC reanalysis.
15 The largest positive anomaly is found over Indonesia in October and November, corresponding
16 to increased aerosol concentrations from biomass burning emissions. The negative aerosol
17 anomaly over South America in October is related to the reduced fire activity seen in Figure
18 23. By December the anomalies have disappeared. Similar AOD anomaly patterns over
19 Indonesia were seen by Tosca et al. (2010) when comparing ~~ELEI~~ Niño and La Niña years for
20 August to October for the period 2000 and 2006 from the MISR and MODIS data.

21 The 3-dimensional nature of the MACC reanalysis allows us to look at the vertical distribution
22 of the anomalies in the troposphere. Figures 89 to 112 show height versus longitude cross-
23 sections of O₃, CO, NO_x and smoke AOD anomalies averaged over the latitude range from 0
24 to 12°S. The O₃ cross section in Figure 89 illustrates that the largest positive O₃ anomalies in
25 October and November are located in the lower troposphere and are likely to be the result of
26 enhanced O₃ production due to increased concentrations of O₃ precursors from enhanced fire
27 emissions. However, the positive and negative anomalies extend into the upper ~~the~~ troposphere,
28 and some of the anomalies (for example the negative anomaly over the Central Pacific) are
29 clearly not connected to the surface but seem to originate in the middle or upper troposphere.
30 These anomalies continue into December after the end of the fire season, and are likely to be a
31 result of the dynamically induced changes mentioned above.

1 Figure 910 shows that CO anomalies are largest in the lower troposphere but can extend
2 throughout the troposphere over Indonesia and South America. There is a clear connection to
3 increased CO emissions over Indonesia and decreased emissions over South America due to
4 changes in biomass burning. By December the anomalies have all but gone and show that there
5 is no dynamically induced anomaly, unlike in O₃. Now a small positive anomaly is found over
6 AfricaSouth America.

7 Figure 1011 shows cross sections of NO_x anomalies calculated from the reanalysis. The largest
8 anomalies are located in the lower troposphere and are again clearly connected to changes in
9 the fire emissions. A large positive anomaly is found over Indonesia and negative anomalies
10 over South America in October and Africa in October and November. In these areas there are
11 reduced fire activities and increased precipitation during El Niño years. Positive NO_x anomalies
12 are found in the upper troposphere and could be a result of increased NO_x production from
13 lightning over South America where there is positive precipitation anomaly pointing to
14 increased convection. The flash rates in the lightning NO parametrization are 5-10 larger over
15 land than over ocean which might explain why no signal is seen over the Central Pacific. The
16 positive NO_x anomalies around 100°E in October and November are collocated with high O₃
17 values in the lower troposphere (Figure 9) pointing to enhanced O₃ production due to enhanced
18 NO_x concentrations from biomass burning. In December, when NO_x does not show such a
19 positive anomaly any more, O₃ concentrations in the lower troposphere are lower and the
20 maximum of the O₃ anomaly is located above 700 hPa.

21 Figure 1112 depicts cross sections of smoke AOD and shows that, as for CO and NO_x, there is
22 a clear connection to increased emissions over Indonesia in October and reduced emissions over
23 South America. By December the positive anomaly over Indonesia is much reduced and
24 confined to the lower troposphere. Enhanced AOD concentrations can be seen in November
25 over South America. In the lower troposphere there is a negative aerosol anomaly over the
26 Central Pacific that is not seen in the other atmospheric composition fields. This anomaly is
27 likely to be the result of the increased precipitation in this area during El Niño conditions (see
28 Figure 1) which leads to increased wet deposition and removal of aerosols, while not removing
29 the gas-phase species in the same way.

30

3 Quantifying the relative importance of dynamically and emission driven changes on the atmospheric composition fields

3.1 Experiment setup

To quantify the relative impact of increased biomass burning emissions and dynamically induced changes on the atmospheric composition fields during El Niño conditions two experiments are run for the years 2005 and 2006: one with normal and one with climatological GFAS v1.0 fire emissions. 2006 was an El Niño year, and 2005 is used to represent normal to weak La Niña conditions. The additional experiments use the most recent version of the MACC system, the C-IFS model (Flemming et al. [2015](#); [Inness et al. 2015](#)). This model is different to the one used in the MACC reanalysis (Inness et al. 2013) because it has chemistry routines included directly in ECMWF's Integrated Forecasting System (IFS). [A basic initial validation of CIFS-fields can be found in Fleming et al. \(2015\) and Inness et al. \(2015\) and more detailed validation of C-IFS can be found in the validation reports available from <http://www.copernicus-atmosphere.eu/>.](#)

The chemistry scheme implemented in the C-IFS model version used for these experiments is an extended, modified version of the Carbon Bond Mechanism 5 (Yarwood et al., 2005) chemical mechanism as originally implemented in the Tracer Model 5 (TM5) CTM (Huijnen et al., 2010, Williams et al., 2013; Huijnen et al., 2014). This is a tropospheric chemistry scheme with 54 species and 126 reactions. For O₃ a simple stratospheric parameterisation based on Cariolle and Teyssèdre (2007) has been added. Monthly mean dry deposition velocities are currently based on climatological fields from MOCAGE (Michou et al., 2004). The module for wet deposition is based on the Harvard wet deposition scheme (Jacob et al., 2000 and Liu et al., 2001). The output of the IFS convection scheme is used to calculate NO emissions from [lightninglightning](#). They are parameterised using estimates of the flash rate density, the flash energy release and the vertical emission profile. Estimates of the flash rate density are based on parameters of the convection scheme and calculated using convective precipitation as input parameter (Meijer et al 2001). Documentation of the technical implementation of C-IFS and more details about the model can be found in Fleming et al. (2015). In the present study, the C-IFS aerosol fields are not used in the radiation scheme, where an aerosol climatology based on Tegen et al. (1997) is used instead. Also, heterogeneous chemistry on aerosols is not included.

1 The anthropogenic emissions used in the C-IFS runs come from the MACCity emission data
2 base (Granier et al., 2011). Biogenic emissions are taken from the POET database for the year
3 2000 (Granier et al. 2005; Olivier et al. 2003), with isoprene emissions from MEGAN2.1, again
4 for the year 2000 (Guenther et al., 2006). Biomass burning emissions for the runs are either
5 taken from GFAS v1.0 (Kaiser et al. 2012) or from a GFAS v1.0 climatology. This daily
6 climatology was constructed using the GFAS v1.0 dataset from 2000 to 2014 (Kaiser et al.
7 2012, Remy and Kaiser, 2014). Biomass burning emissions for each day of the year were
8 defined as the average of the emissions of the same day of the year for the 15 years of the
9 dataset.

10 The differences between the GFAS v1.0 and climatological GFAS emissions for the area
11 between 10°N, 10°S, 90°E, 130°E are shown in Figure 4213. The figure illustrates that 2006
12 was a year with exceptionally large biomass burning emissions over Indonesia during the
13 biomass burning season (as already seen in Figure 45), while in 2005 emissions were slightly
14 below average.

15 The experiments are started on 1 January 2005 and run until the end of 2006. The first
16 experiment (BASE) uses daily GFAS v1.0 emissions, while the second experiment (CLIM)
17 uses the climatological GFAS data set described above. We look at fields from these
18 experiments for October and December 2005 and 2006 to determine

- 19 i. the overall impact of changes to the atmospheric composition fields due to El Niño
20 related dynamically and emission induced changes by comparing BASE for the years
21 2006 and 2005 (BASE06 minus BASE05),
- 22 ii. changes of atmospheric composition due to differences in the biomass burning
23 emissions under El Niño conditions by comparing BASE and CLIM for 2006 (BASE06
24 minus CLIM06),
- 25 iii. the impact of the El Niño induced dynamical changes on atmospheric composition and
26 O₃ production by comparing CLIM for the years 2006 and 2005 (CLIM06 minus
27 CLIM05).

28

1 3.2 Results of the C-IFS experiments

2 Figure 4314 shows timeseries of the tropospheric CO, O₃ and NO₂ burdens from the BASE and
3 CLIM experiments averaged over the area between 10°N, 10°S, 90°E, 130°E. Between
4 September and November 2006 the GFAS v1.0 fire emissions used in BASE lead to an
5 increased CO burden, which reaches values up to 21 Tg, almost double the values seen in CLIM
6 (around 11 Tg). In 2005 the tropospheric CO burden in both experiments is similar to the CLIM
7 values of 2006 (around 10-12 Tg). Tropospheric O₃ burdens show a smaller increase (about
8 8%) in 2006 from about 7.4 Tg in CLIM to 8 Tg in BASE. The 2006 O₃ burdens in BASE are
9 increased by about 30% relative to 2005, when the tropospheric O₃ burden is about 6 Tg in both
10 experiments. It should be noted that the tropospheric O₃ mass shows considerable intra seasonal
11 fluctuations. The tropospheric NO₂ burden in BASE is increased by about 20-30% compared
12 to CLIM in September 2006 as a result of the increased fire emissions. During 2005 NO₂
13 burdens from BASE and CLIM are of similar magnitude.

14 The top panels of Figure 4415 show the overall impact of changes to the tropospheric O₃ column
15 due to dynamically and emission driven changes, by comparing BASE06 and BASE05 for
16 October and December. The patterns are very similar to the ones seen in the MACC reanalysis
17 composite O₃ anomalies at 500 hPa (Figure 45). The combined effect of dynamically induced
18 and emission driven changes leads to an increase of TCO₃ by over 50% in a large area
19 ~~surroundingsurrounding~~ Indonesia and to a reduction of 10-30% over large parts of the Central
20 Pacific. TCO₃ values are also reduced by more than 30% over Brazil. TCO₃ changes due to
21 changes in the fire emissions alone (middle panels of Figure 4415) can only explain part of the
22 observed O₃ increase over Indonesia (which is consistent with the small differences between
23 BASE and CLIM seen in Figure 4314 for September to November 2006) and a small decrease
24 over Brazil, and can not explain the reduction of O₃ over the Pacific. The dynamically induced
25 changes in October (Figure 4415, bottom left) show a similar pattern to the overall differences
26 between El Niño and normal conditions. This illustrates that while emission driven changes can
27 explain about half of the total TCO₃ changes in a small area surrounding Indonesia, the TCO₃
28 increase outside this region and the negative O₃ anomaly over the Pacific is unrelated to changes
29 in the fire emissions. This is also confirmed by the December plots, when no fire related
30 anomaly is seen any more (Figure 4415, middle right). The dynamically driven O₃ anomalies
31 persist into December and can explain most of the TCO₃ anomaly (Figure 4415, bottom right).

1 Over Indonesia the O₃ maxima are now located around 10°N and 10°S, and over the Pacific
2 they are slightly smaller scale than in October.

3 The importance of the dynamically driven ozone changes was also highlighted by Lin et al.
4 (2014 and 2015). Despite large El Nino enhancements to wildfire activity in equatorial Asia,
5 the model sensitivity experiments in Lin et al. (2014) indicated that wildfire emissions are not
6 the main driver of ENSO-related ozone variability observed at Mauna Loa, Hawaii. The
7 dynamically induced eastward extension and equatorward shift of the subtropical jet stream
8 during El Nino plays a key role on observed interannual variability of springtime lower
9 tropospheric ozone at Mauna Loa. These shifts enhance long range transport of Asian ozone
10 and CO pollution towards the eastern North Pacific in winter and spring during El Nino. Lin et
11 al. (2015) demonstrated a connection between springtime western US ozone air quality and jet
12 characteristics associated with strong La Nina winters. They showed more frequent late spring
13 deep stratospheric ozone intrusions when the polar jet stream meanders southward over the
14 western United States as occurs following strong La Nina winters.

15 The TCO₃ changes seen in the bottom panel of Figure 4415 are anti-correlated with changes in
16 specific humidity (Figure 4516, top panels) pointing to an enhanced O₃ lifetime over Indonesia
17 due to reduced humidity and hence OH concentrations. Furthermore, there is enhanced ascent
18 over the Central Pacific and enhanced descent over Indonesia (Figure 4516, bottom panels) so
19 that increased upward transport of clean O₃ poor air over the Pacific and increased downward
20 transport from the upper troposphere/stratosphere in the Indonesian region will also affect the
21 tropospheric O₃ columns. In October the peak in specific humidity is located south of the ozone
22 enhancement. This agrees with Nassar et al. (2009) who showed that the equatorial component
23 of the October ozone anomaly was related to fire emissions, while the southern component of
24 the ozone anomaly was due to other factors. It should be noted that the positive specific
25 humidity anomalies over the Arabian peninsula and over Australia in October do not correspond
26 to decreased ozone values, while the ones over southern Africa, South America and the Central
27 Pacific do. The reason for this is that relative anomalies are shown and that the absolute
28 humidity values over the Arabian peninsula and Australia are much lower than in the other
29 areas, so that the absolute humidity changes between 2006 and 2005 are actually relatively
30 small. This all suggests that the correlation of O₃ to specific humidity is strongest in tropical
31 regions with large variability in water vapour, combined with low NO_x conditions.

1 Figure 4617 shows that the TCCO anomalies over Indonesia are almost entirely emission
2 driven, in contrast to the TCO3 anomalies seen in Figure 4415. Using GFAS v1.0 emissions
3 rather than climatological GFAS emissions can explain most of the TCCO anomaly over
4 Indonesia in October, apart from two small positive dynamically induced anomalies to the east
5 and west of the maritime continent. By December, after the end of the fire season in Indonesia,
6 the TCCO anomalies have almost gone.

7 As for CO, the NO₂ and smoke aerosol anomalies are entirely emission driven (not shown). For
8 both these fields, no anomalies are seen when comparing CLIM06 and CLIM05, and the
9 anomalies seen when comparing BASE06 and BASE05 are gone by December. It is possible
10 that we would also see some dynamically induced changes in the smoke aerosols if aerosols
11 were interactive with the radiation scheme in the model runs. However, without this feedback
12 the smoke aerosol anomalies are entirely emission driven.

13 Figure 4718 shows O₃-CO correlations for October 2005 and 2006 from the BASE and CLIM
14 experiments. We focus only on October as the month with the largest anomaly in the fire
15 emissions. Such correlations have been used in several studies (e.g., Kim et al., 2013,
16 Voulgarakis et al., 2011 and references therein) going back to Fishman and Seiler (1983) to
17 identify regions of photochemically produced O₃ (positive correlations) and O₃ from other
18 sources (e.g. downward transport from stratosphere) as well as O₃ loss due to chemistry or
19 deposition (negative correlations). In 2005, free tropospheric O₃-CO correlations (Figure 4718
20 a and c) show a similar distribution across the Maritime Continent with relatively weak ($r <$
21 0.7) negative correlations extending from the Indian Ocean south of Indonesia to East and West
22 Malaysia and the Philippines, and positive correlations over northern and eastern Indonesia.
23 Slight differences in the distribution of the O₃-CO correlations between Figure 4718 (a) and (c)
24 reflect differences in the fire emissions between the BASE and CLIM experiments. Larger
25 differences are seen in the distribution of free tropospheric O₃-CO correlations between BASE
26 and CLIM for the El Nino year of 2006 (Figure 4718 b and d). The increased fire activity in
27 2006 (Figures 4 and 4213) gives rise to larger positive ($r > 0.7$) O₃-CO correlations extending
28 across most of Indonesia and Malaysia in the BASE experiment (Figure 47b18b) and reflect
29 enhanced O₃ photochemistry associated with increased emissions of O₃ precursors from the
30 fires. This agrees well with the area of increased O₃ concentrations due to fires seen in Figure
31 16 when comparing BASE06 and CLIM06. In contrast, O₃-CO correlations in the CLIM
32 experiment (Figure 47d18d) are generally negative over much of Indonesia and Malaysia and

1 reflect the influence of transport across the region and the lack of enhanced O₃ production when
2 the climatological fire emissions are used.

3

4 **4 Conclusions and outlook**

5 In this paper O₃, CO, NO₂ and smoke aerosol fields from the MACC reanalysis (Inness et al.,
6 2013) were used to identify the ENSO signal in tropical atmospheric composition fields,
7 concentrating on the months September to December. The MACC atmospheric composition
8 fields show a clear ENSO related anomaly signal with increased O₃, CO, NO₂ and smoke
9 aerosols over the Maritime Continent during El Niño years. O₃ also shows larger scale changes
10 with decreased tropospheric columns over the Central and Eastern Pacific and increased
11 columns over the Western Pacific and the Maritime continent that continue after the end of the
12 Indonesian fire season.

13 Two simulations were carried out with the C-IFS model to quantify to what extent the ENSO
14 signal seen in the atmospheric composition fields was due to changes in the biomass burning
15 emissions or due to dynamically induced changes, e.g. related to changes in the vertical
16 transport of O₃ from the lower troposphere and the stratosphere, and to changes of the photolysis
17 of O₃ due to changes to OH. While the CO, NO₂ and smoke aerosol changes were almost
18 entirely driven by changes in biomass burning emissions due to increased wild fires over the
19 Maritime Continent during El Niño related drought conditions, changes in tropospheric O₃ were
20 largely dynamically induced and only to a small part driven by changes in the emissions. The
21 emission driven O₃ changes were confined to the area surrounding Indonesia, where enhanced
22 photochemical O₃ production occurs under El Niño conditions because of increased biomass
23 burning activities, while the larger-scale O₃ anomalies were dynamically induced.

24 ~~Comparing~~ Comparing simulations with daily GFAS v1.0 emissions for the years 2005 and
25 2006 and a daily GFAS v1.0 climatology of the period 2000 to 2014 showed that tropospheric
26 CO was almost doubled in September 2006 relative to September 2005 due to increased fire
27 emissions, NO₂ was increased by 20-30 % and O₃ by about 8%. For tropospheric O₃,
28 dynamically induced changes dominated the differences between 2006 and 2005. The fire
29 induced O₃ anomaly was smaller in magnitude and horizontal extent than the dynamically
30 induced changes which ~~affeced~~ affected much of the Tropics. In 2006, tropospheric O₃ was
31 increased by more than 50% over the Maritime Continent and Indian Ocean compared to 2005,

1 and decreased by between 20-30 % over large parts of the Tropical Pacific when the same
2 climatological fire emissions were used in both years. Only in a small area over Indonesia was
3 the O₃ increase due to fires of similar magnitude to the dynamically induced changes. A future
4 study will look in more detail at the chemistry budgets and chemical processes that cause the
5 changes in the atmospheric composition fields.

6 The results from this paper show that the MACC system is able to ~~successfully~~ model ~~the ENSO~~
7 ~~signal changes~~ in atmospheric composition fields found under El Niño and La Niña
8 conditions. After a more thorough validation of the MACC atmospheric fields against
9 observations, it could ~~therefore~~ be ~~used in further studies~~ interesting to investigate the ocean-

10 atmosphere response to ENSO induced changes in atmospheric composition in a further study.

11 A first step would be to include the aerosol direct and indirect effects through the cloud
12 microphysics in the radiation scheme of the IFS and to look at the feedback of fire-induced
13 aerosols on climate. We would expect a positive feedback, i.e. reduced convection due to
14 increased atmospheric stability, as carbonaceous aerosols usually absorb (and thus re-emit) a
15 significant amount of solar radiation in the mid troposphere, and increased aerosol
16 concentrations also lead to reduced land and sea surface temperatures. Their presence should
17 therefore act to reduce convection and precipitation over the Maritime Continent. Including the
18 aerosols in the radiation scheme will also affect the chemical fields through changes in the UV
19 radiation and hence photolysis rates. A second step could see the coupling of the chemistry and
20 aerosol fields by including heterogeneous chemistry on aerosols. In a final step it can be
21 envisaged to fully couple the MACC system with ECMWF's ocean model to investigate how
22 the forcing from ENSO induced changes to atmospheric composition fields can feedback on
23 the ENSO dynamics.

24 MACC atmospheric composition data are freely available from [www.copernicus-](http://www.copernicus-atmosphere.eu)
25 [atmosphere.eu](http://www.copernicus-atmosphere.eu).

26

27 **Acknowledgements**

28 MACC-II was funded by the European Commission under the EU Seventh Research
29 Framework Programme, contract number 283576. MACC-III was funded by the European
30 Commission under Horizon2020 as a Coordination & Support Action, grant agreement number
31 633080.

1

2 **References**

3 Allan, R. J., Lindesay, J. and Parker D. E.: El Niño Southern Oscillation and climatic variability.
4 416 pages, CSIRO Publishing, Collingwood, Victoria, Australia, ISBN: 9780643058033, 1996.

5 Aouizerats, B., van der Werf, G. R., Balasubramanian, R., and Betha, R.: Importance of
6 transboundary transport of biomass burning emissions to regional air quality in Southeast Asia
7 during a high fire event, *Atmos. Chem. Phys.*, 15, 363-373, doi:10.5194/acp-15-363-2015,
8 2015.

9 Barkley, M.: Description of MEGAN biogenic VOC emissions in GEOS-Chem, available at:
10 http://acmg.seas.harvard.edu/geos/wiki_docs/emissions/megan.pdf (last access 11 May 2015),
11 2010.

12 Benedetti, A., Morcrette, J.-J., Boucher, O., Dethof, A., Engelen, R. J., Fisher, M., Flentje, H.,
13 Huneeus, N., Jones, L., Kaiser, J. W., Kinne, S., Mangold, A., Razinger, M., Simmons, A. J.,
14 Suttie, M., and the GEMS-AER team: Aerosol analysis and forecast in the European Centre for
15 Medium-Range Weather Forecasts Integrated Forecast System: 2. Data assimilation, *J.*
16 *Geophys. Res.*, 114, D13205, doi:10.1029/2008JD011115, 2009.

17 Chandra, S., Ziemke, J. R., Duncan, B. N., Diehl, T. L., Livesey, N. J., and Froidevaux, L.:
18 Effects of the 2006 El Niño on tropospheric ozone and carbon monoxide: implications for
19 dynamics and biomass burning, *Atmos. Chem. Phys.*, 9, 4239-4249, doi:10.5194/acp-9-4239-
20 2009, 2009.

21 Cariolle, D. and Teyssède, H.: A revised linear ozone photochemistry parameterization for
22 use in transport and general circulation models: multi-annual simulations. *Atmos. Chem. Phys.*,
23 7, 2183-2196, 2007.

24 Chandra, S., Ziemke, J. R., Schoeberl, M. R., Froidevaux, L., Read, W. G., Levelt, P. F. and
25 Bhartia, P. K.: Effects of the 2004 El Niño on tropospheric ozone and water vapour. *Geophys.*
26 *Res. Lett.*, 34, L06802, doi:10.1029/2006GL028779, 2007.

27 Chandra, S., Ziemke, J. R., Bhartia, P. K. and Martin, R. V.: Tropical tropospheric ozone:
28 Implications for dynamics and biomass burning, *J. Geophys. Res.*, 107(D14),
29 doi:10.1029/2001JD000447, 2002.

1 Chandra, S., Ziemke, J.R, Min, W. and Read, W.G.: Effects of 1997-1998 El Niño on
2 tropospheric ozone. *Geophys. Res. Lett.*, vol. 25, 20, 3867-3870, 1998.

3 Chung, C. E. and Ramanathan, V.: South Asian haze forcing: Remote impacts with implications
4 to ENSO and AO. *Journal of Climate*, 16(11), 1791-1806, 2003.

5 Dee, D. P., Uppala, S. M., Simmons, A. J., Berrisford, P., Poli, P., Kobayashi, S., Andrae, U.,
6 Balmaseda, M. A., Balsamo, G., Bauer, P., Bechtold, P., Beljaars, A. C. M., van de Berg, L.,
7 Bidlot, J., Bormann, N., Delsol, C., Dragani, R., Fuentes, M., Geer, A. J., Haimberger, L.,
8 Healy, S. B., Hersbach, H., Hólm, E. V., Isaksen, L., Kallberg, P., Köhler, M., Matricardi,
9 M., McNally, A. P., Monge-Sanz, B. M., Morcrette, J.-J., Park, B.-K., Peubey, C., de Rosnay,
10 P., Tavolato, C., Thépaut, J.-N., and Vitarta, F.: The ERA-Interim reanalysis: configuration
11 and performance of the data assimilation system, *Q. J. Roy. Meteor. Soc.*, 137, 553–597, 2011.

12 Dentener, F., Kinne, S., Bond, T., Boucher, O., Cofala, J., Generoso, S., Ginoux, P., Gong, S.,
13 Hoelzemann, J. J., Ito, A., Marelli, L., Penner, J. E., Putaud, J.-P., Textor, C., Schulz, M., van
14 der Werf, G. R., and Wilson, J.: Emissions of primary aerosol and precursor gases in the years
15 2000 and 1750 prescribed data-sets for AeroCom, *Atmos. Chem. Phys.*, 6, 4321-4344,
16 doi:10.5194/acp-6-4321-2006, 2006.

17 Duncan, B. N., Bey, I., Chin, M., Mickley, L. J. , Fairlie, T. D., Martin, R. V. and Matsueda,
18 H.: Indonesian wildfires of 1997: Impact on tropospheric chemistry, *J. Geophys. Res.*, 108,
19 4458, doi:10.1029/2002JD003195, D15, 2003.

20 Doherty, R. M., Stevenson, D. S., Johnson, C. E., Collins, W. J., and Sanderson, M. G.:
21 Tropospheric ozone and El Niño–Southern Oscillation: Influence of atmospheric dynamics,
22 biomass burning emissions, and future climate change. *J. Geophys. Res.*, 111, D19304,
23 doi:10.1029/2005JD006849, 2006.

24 Fishman, J., and Seiler, W.: Correlative nature of ozone and carbon monoxide in the
25 troposphere: Implications for the tropospheric ozone budget, *J. Geophys. Res.*, 88(C6), 3662–
26 3670, doi:10.1029/JC088iC06p03662, 1983.

27 Flemming, J., Huijnen, V., Arteta, J., Bechtold, P., Beljaars, A., Blechschmidt, A.-M.,
28 Diamantakis, M., Engelen, R. J., Gaudel, A., Inness, A., Jones, L., Josse, B., Katragkou, E.,
29 Marecal, V., Peuch, V.-H., Richter, A., Schultz, M. G., Stein, O., and Tsikerdekis, A.:

1 Tropospheric chemistry in the Integrated Forecasting System of ECMWF, *Geosci. Model Dev.*,
2 8, 975-1003, doi:10.5194/gmd-8-975-2015, 2015.

3 Fujiwara, M., Kita, K., Kawakami, S., Ogawa, T., Komala, N., Saraspriya, S. and Suropto, A.:
4 Tropospheric ozone enhancements during the Indonesian forest fire events in 1994 and in 1997
5 as revealed by ground-based observations, *Geophys. Res. Lett.*, 26, 2417–2420, 1999.

6 Granier, C., Bessagnet, B., Bond, T., D'Angiola, A., Denier van der Gon, H., Frost, G. J., Heil,
7 A., Kaiser, J. W., Kinne, S., Klimont, Z., Kloster, S., Lamarque, J.-F., Liousse, C., Masui, T.,
8 Meleux, F., Mieville, A., Ohara, R., Raut, J.-C., Riahi, K., Schultz, M. G., Smith, S. G.,
9 Thompson, A., van Aardenne, J., van der Werf, G. R., and van Vuuren, D. P.: Evolution of
10 anthropogenic and biomass burning emissions of air pollutants at global and regional scales
11 during the 1980-2010 period. *Climatic Change*, 109, 163-190. DOI: 10.1007/s 10584-011-
12 0154-1, 2011.

13 Granier, C., Guenther, A., Lamarque, J., Mieville, A., Muller, J., Olivier, J., Orlando, J., Peters,
14 J., Petron, G., Tyndall, G., and Wallens, S.: POET, a database of surface emissions of ozone
15 precursors, available at: <http://www.aero.jussieu.fr/projet/ACCENT/POET.php> (last access:
16 December 2014), 2005.

17 Guenther, A., Karl, T., Harley, P., Wiedinmyer, C., Palmer, P.I., and Geron, C.: Estimates of
18 global terrestrial isoprene emissions using MEGAN (Model of Emissions of Gases and
19 Aerosols from Nature), *Atmos. Chem. Phys.*, 6, 3181-3210, 2006.

20 Hauglustaine, D. A., Brasseur, G. P. , Walters, S., Rasch, P. J., Müller, J.-F., Emmons, L. K.
21 and Carroll, M. A.: MOZART, a global chemical transport model for ozone and related
22 chemical tracers, 2, Model results and evaluation, *J. Geophys. Res.*, 103, 28291–28335, 1999.

23 Huijnen, V., Williams, J. E., and Flemming, J.: Modeling global impacts of heterogeneous loss
24 of HO₂ on cloud droplets, ice particles and aerosols, *Atmos. Chem. Phys. Discuss.*, 14, 8575-
25 8632, doi:10.5194/acpd-14-8575-2014, 2014.

26 Huijnen, V., Williams, J., van Weele, M., van Noije, T., Krol, M., Dentener, F., Segers, A.,
27 Houweling, S., Peters, W., de Laat, J., Boersma, F., Bergamaschi, P., van Velthoven, P., Le
28 Sager, P., Eskes, H., Alkemade, F., Scheele, R., Nédélec, P., and Pätz, H.-W.: The global
29 chemistry transport model TM5: description and evaluation of the tropospheric chemistry
30 version 3.0, *Geosci. Model Dev.*, 3, 445-473, doi:10.5194/gmd-3-445-2010.

1 [Inness, A., Blechschmidt, A.-M., Bouarar, I., Chabrillat, S., Crepulja, M., Engelen, R. J., Eskes,](#)
2 [H., Flemming, J., Gaudel, A., Hendrick, F., Huijnen, V., Jones, L., Kapsomenakis, J.,](#)
3 [Katragkou, E., Keppens, A., Langerock, B., de Mazière, M., Melas, D., Parrington, M., Peuch,](#)
4 [V. H., Razinger, M., Richter, A., Schultz, M. G., Suttie, M., Thouret, V., Vrekoussis, M.,](#)
5 [Wagner, A., and Zerefos, C.: Data assimilation of satellite-retrieved ozone, carbon monoxide](#)
6 [and nitrogen dioxide with ECMWF's Composition-IFS, *Atmos. Chem. Phys.*, **15**, 5275-5303,](#)
7 [doi:10.5194/acp-15-5275-2015, 2015.](#)

8 Inness, A., Baier, F., Benedetti, A., Bouarar, I., Chabrillat, S., Clark, H., Clerbaux, C., Coheur,
9 P., Engelen, R. J., Errera, Q., Flemming, J., George, M., Granier, C., Hadji-Lazaro, J., Huijnen,
10 V., Hurtmans, D., Jones, L., Kaiser, J. W., Kapsomenakis, J., Lefever, K., Leitão, J., Razinger,
11 M., Richter, A., Schultz, M. G., Simmons, A. J., Suttie, M., Stein, O., Thépaut, J.-N., Thouret,
12 V., Vrekoussis, M., Zerefos, C., and the MACC team: The MACC reanalysis: an 8 yr data set
13 of atmospheric composition, *Atmos. Chem. Phys.*, **13**, 4073-4109, doi:10.5194/acp-13-4073-
14 2013, 2013.

15 Jacob, D.J., Liu, H., Mari, C. and Yantosca, R.M.: Harvard wet deposition scheme for GMI,
16 Harvard University Atmospheric Chemistry Modeling Group, revised March 2000.
17 http://acmg.seas.harvard.edu/geos/wiki_docs/deposition/wetdep.jacob_etal_2000.pdf (last
18 access December 2014), 2000.

19 Kaiser, J. W., Heil, A., Andreae, M. O., Benedetti, A., Chubarova, N., Jones, L., Morcrette, J.-
20 J., Razinger, M., Schultz, M. G., Suttie, M., and van der Werf, G. R.: Biomass burning
21 emissions estimated with a global fire assimilation system based on observed fire radiative
22 power. *Biogeosciences*, **9**:527–554, 2012.

23 [Meiyun Lin, A.M. Fiore, L.W. Horowitz, A.O.Langford, S. J. Oltmans, D. Tarasick, H.E.](#)
24 [Reider \(2015\): Climate variability modulates western US ozone air quality in spring via deep](#)
25 [stratospheric intrusions, *Nature Communications*, **6**, 7105, doi:10.1038/ncomms8105](#)

26 [Meiyun Lin, L.W. Horowitz, S. J. Oltmans, A. M. Fiore, Songmiao Fan \(2014\): Tropospheric](#)
27 [ozone trends at Manna Loa Observatory tied to decadal climate variability, *Nature Geoscience*,](#)
28 [7, 136-143, doi:10.1038/NGEO2066.](#)

29 Liu, H., Jacob, D.J., Bey, I., Yantosca, R.M.: Constraints from ²¹⁰Pb and ⁷Be on wet
30 deposition and transport in a global three-dimensional chemical tracer model driven by
31 assimilated meteorological fields. *Journal of Geophysical Research* **106**, 12109e12128, 2001.

1 Logan, J. A., Megretskaia, I., Nassar, R., Murray, L. T., Zhang, L., Bowman, K. W., Worden,
2 H. M. and Luo, M.: Effects of the 2006 El Niño on tropospheric composition as revealed by
3 data from the Tropospheric Emission Spectrometer (TES), *Geophys. Res. Lett.*, 35, L03816,
4 doi:10.1029/2007GL031698, 2008.

5 Lyon, B.: The strength of El Niño and the spatial extent of tropical drought, *Geophys. Res.*
6 *Lett.*, 31, L21204, doi:10.1029/2004GL020901, 2004.

7 Meijer, E.W., van Velthoven, P. F. J., Brunner, D. W., Huntrieser, H. and Kelder, H.:
8 Improvement and evaluation of the parameterisation of nitrogen oxide production by lightning,
9 *Physics and Chemistry of the Earth, Part C, Volume 26, Issue 8, Pages 577-583*, 2001.

10 Michou M., Laville, P., Serça, D., Fotiadi, A., Bouchou P., and Peuch, V.-H.: Measured and
11 modeled dry deposition velocities over the ESCOMPTE area, *Atmos. Res.*, 74 (1-4), 89- 116,
12 2004.

13 Morcrette, J.-J., Benedetti, A., Jones, L., Kaiser, J. W., Razinger, M. and Suttie, M.: Prognostic
14 aerosols in the ECMWF IFS: MACC vs GEMS aerosols. ECMWF RD Tech. Memo. 659, 2011.
15 Available from [http://old.ecmwf.int/publications/library/ecpublications/_pdf/tm/601-](http://old.ecmwf.int/publications/library/ecpublications/_pdf/tm/601-700/tm659.pdf)
16 [700/tm659.pdf](http://old.ecmwf.int/publications/library/ecpublications/_pdf/tm/601-700/tm659.pdf) (last access January 2015)

17 Nassar, R., Logan, J. A., Megretskaia, I. A., Murray, L. T., Zhang, L. and Jones, D. B. A.:
18 Analysis of tropical tropospheric ozone, carbon monoxide, and water vapor during the 2006 El
19 Niño using TES observations and the GEOS-Chem model, *J. Geophys. Res.*, 114, D17304,
20 doi:10.1029/2009JD011760, 2009.

21 Olivier, J., Peters, J., Granier, C., Petron, G., Müller, J., and Wallens, S.: Present and future
22 surface emissions of atmospheric compounds, POET report #2, EU project EVK2-1999-
23 00011, available at, <http://www.aero.jussieu.fr/projet/ACCENT/POET.php> (last access
24 December 2014), 2003.

25 Page, S. E., Siegert, F., Rieley, J. O., Boehm, H. D., Jaya, A., and Limin, S.: The amount of
26 carbon released from peat and forest fires in Indonesia during 1997, *Nature*, 420, 61–65,
27 doi:10.1038/nature01131, 2002.

28 [Paugam, R., Wooster, M., Atherton, J., Freitas, S. R., Schultz, M. G., and Kaiser, J. W.:](#)
29 [Development and optimization of a wildfire plume rise model based on remote sensing data](#)

1 [inputs – Part 2, Atmos. Chem. Phys. Discuss., 15, 9815-9895, doi:10.5194/acpd-15-9815-2015,](#)
2 [2015.](#)

3 Podgorny, I. A., Li, F. and Ramanathan, V.: Large Aerosol Radiative Forcing due to the 1997
4 Indonesian Forest Fire, *Geophys. Res. Lett.*, 30, 1028, doi:10.1029/2002GL015979, 2003.

5 Remy, S. and Kaiser, J. W.: Daily global fire radiative power fields estimation from one or two
6 MODIS instruments, *Atmos. Chem. Phys.*, 14, 13377-13390, doi:10.5194/acp-14-13377-2014,
7 2014.

8 Sudo, K. and Takahashi, M.: Simulation of tropospheric ozone changes during 1997-1998 El
9 Niño: Meteorological impact on tropospheric photochemistry, *Geophys. Res. Lett.*, 28, 4091–
10 4094, 2001.

11 Tegen, I., Hollrig, P., Chin, M., Fung, I., Jacob, D. and Penner, J.: Contribution of different
12 aerosol species to the global aerosol extinction optical thickness: Estimates from model results,
13 *J. Geophys. Res.*, 102, 23,895-23,915, 1997.

14 Tosca, M. G., Randerson, J. T., Zender, C. S., Flanner, M. G., and Rasch, P. J.: Do biomass
15 burning aerosols intensify drought in equatorial Asia during El Niño? *Atmos. Chem. Phys.*, 10,
16 3515-3528, doi:10.5194/acp-10-3515-2010, 2010.

17 van der Werf, G. R., Randerson, J. T., Giglio, L., Collatz, G. J., Mu, M., Kasibhatla, P. S.,
18 Morton, D. C., DeFries, R. S., Jin, Y., and van Leeuwen, T. T.: Global fire emissions and the
19 contribution of deforestation, savanna, forest, agricultural, and peat fires (1997–2009), *Atmos.*
20 *Chem. Phys.*, 10, 11707–11735, doi:10.5194/acp-10-11707-2010, 2010.

21 van der Werf, G. R., Randerson, J. T., Giglio, L., Collatz, G. J., Kasibhatla, P. S., and Arellano
22 Jr., A. F.: Interannual variability in global biomass burning emissions from 1997 to 2004,
23 *Atmos. Chem. Phys.*, 6, 3423-3441, doi:10.5194/acp-6-3423-2006, 2006.

24 [Veira, A., Kloster, S., Schutgens, N. A. J., and Kaiser, J. W.: Fire emission heights in the climate](#)
25 [system – Part 2: Impact on transport, black carbon concentrations and radiation, Atmos. Chem.](#)
26 [Phys., 15, 7173-7193, doi:10.5194/acp-15-7173-2015, 2015.](#)

27 Voulgarakis, A., Savage, N. H., Wild, O., Braesicke, P., Young, P. J., Carver, G. D., and Pyle,
28 J. A.: Interannual variability of tropospheric composition: the influence of changes in
29 emissions, meteorology and clouds, *Atmos. Chem. Phys.*, 10, 2491-2506, doi:10.5194/acp-10-
30 2491-2010, 2010.

- 1 Wang, Y., Field, R. D. and Roswintiarti, O.: Trends in atmospheric haze induced by peat fires
2 in Sumatra Island, Indonesia and El Niño phenomenon from 1973 to 2003, *Geophys. Res. Lett.*,
3 31, L04103, doi:10.1029/2003GL018853, 2004.
- 4 Ziemke, J. R. and Chandra, S.: La Niña and El Niño—induced variabilities of ozone in the
5 tropical lower atmosphere during 1970–2001, *Geophys. Res. Lett.*, 30, 1142,
6 doi:10.1029/2002GL016387, 3, 2003.
- 7 Ziemke, J. R. and Chandra, S.: Seasonal and interannual variabilities in tropical tropospheric
8 ozone, *J. Geophys. Res.*, 104(D17), 21425–21442, doi:10.1029/1999JD900277, 1999.
9

1 **5 Tables**

2

3 Table 1: Biomass burning emissions in Tg per month for CO, NO_x, and the smoke aerosols
 4 (sum of organic matter and black carbon) from GFAS v1.0 for the region 10°N - 10°S, 90°E -
 5 130°E averaged over the El Niño years (2004, 2006, 2009) and the La Niña years (2005, 2007,
 6 2008, 2010, 2011), as well as the ratio of the El Niño/ La Niña values.

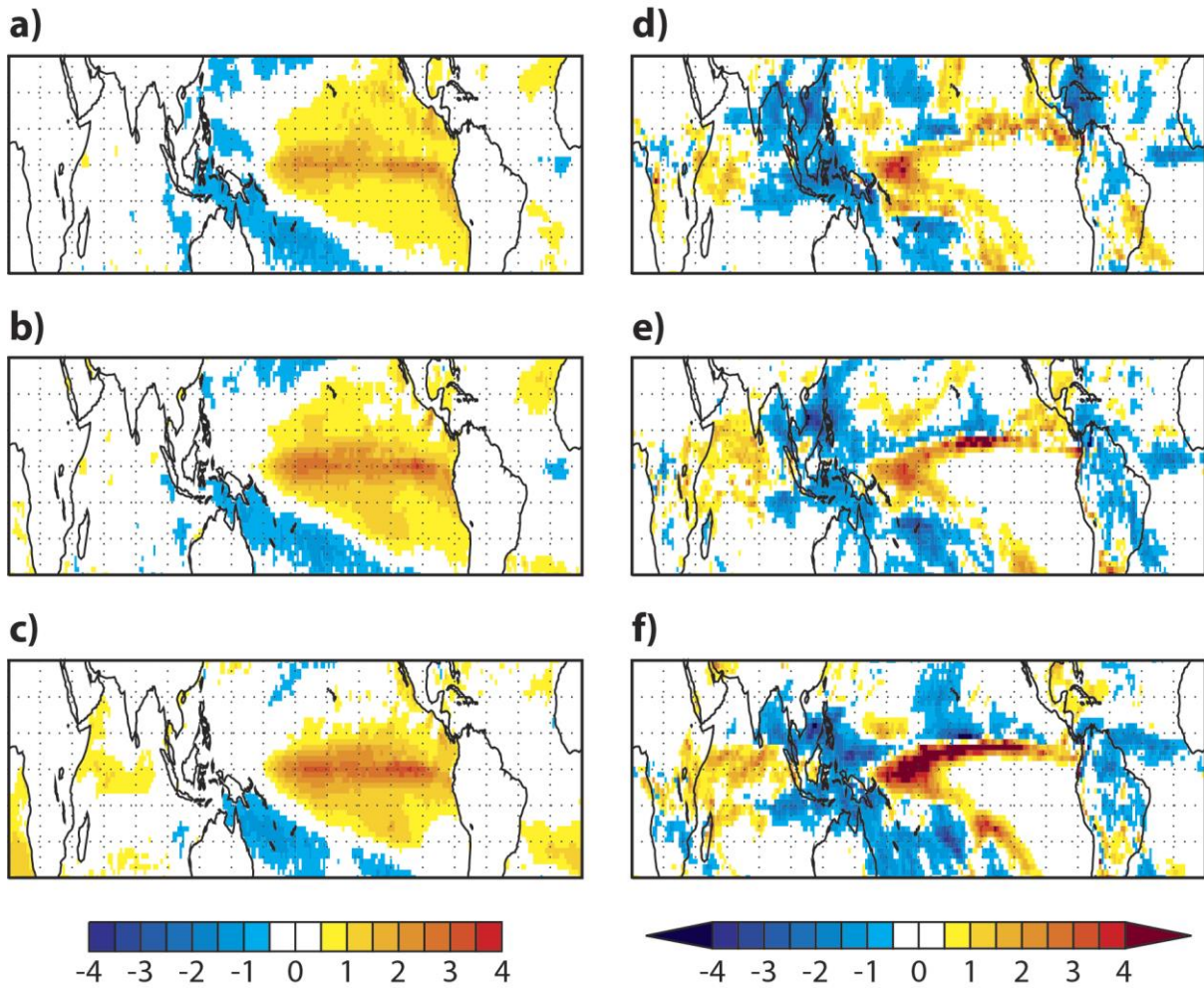
	CO	CO	CO	NO_x	NO_x	NO_x	OM+BC	OM+BC	OM+BC
	Oct	Nov	Dec	Oct	Nov	Dec	Oct	Nov	Dec
El Niño	13.9	3.0	2.4 10 ⁻¹	8.4 10 ⁻²	1.9 10 ⁻²	2.8 10 ⁻³	6.3 10 ⁻¹	1.4 10 ⁻¹	1.3 10 ⁻²
La Niña	1.5	2.5 10 ⁻¹	1.4 10 ⁻¹	1.4 10 ⁻²	3.0 10 ⁻³	1.5 10 ⁻³	7.3 10 ⁻²	1.4 10 ⁻²	7.3 10 ⁻³
El Niño/ La Niña	9.5	11.8	1.7	6.1	6.3	1.9	8.6	10.0	1.8

7

8

1

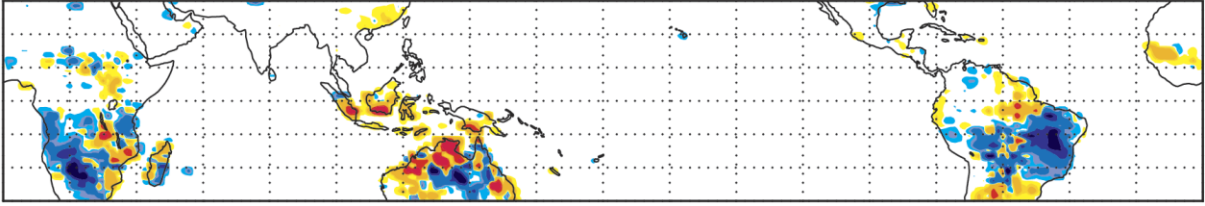
2 **6 Figures**



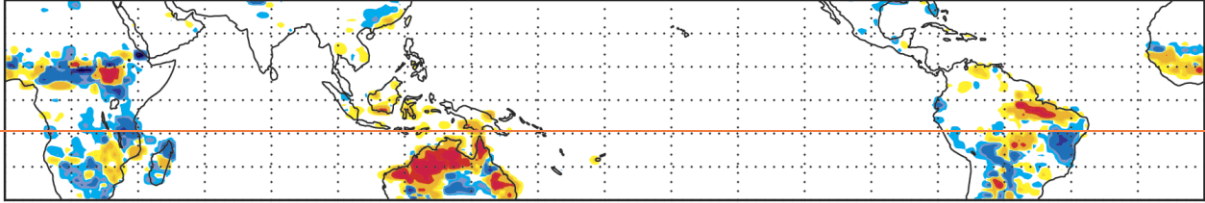
3

4 Figure 1: Left panels: SST anomaly in K calculated from ERA Interim as the difference of El
5 Niño composite minus La Niña composite for October (a), November (b) and December (c).
6 Right panels: Precipitation anomaly in mm/day calculated from ERA Interim as the difference
7 of El Niño composite minus La Niña composite for October (d), November (e) and December
8 (f). Red colours indicate positive values, blue colours negative values.

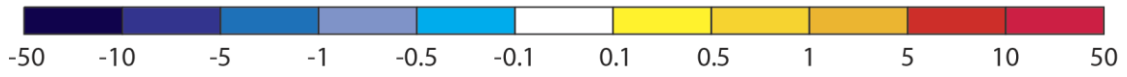
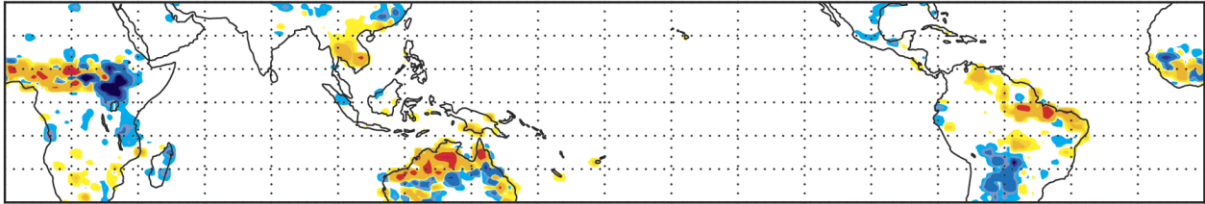
a)



b)



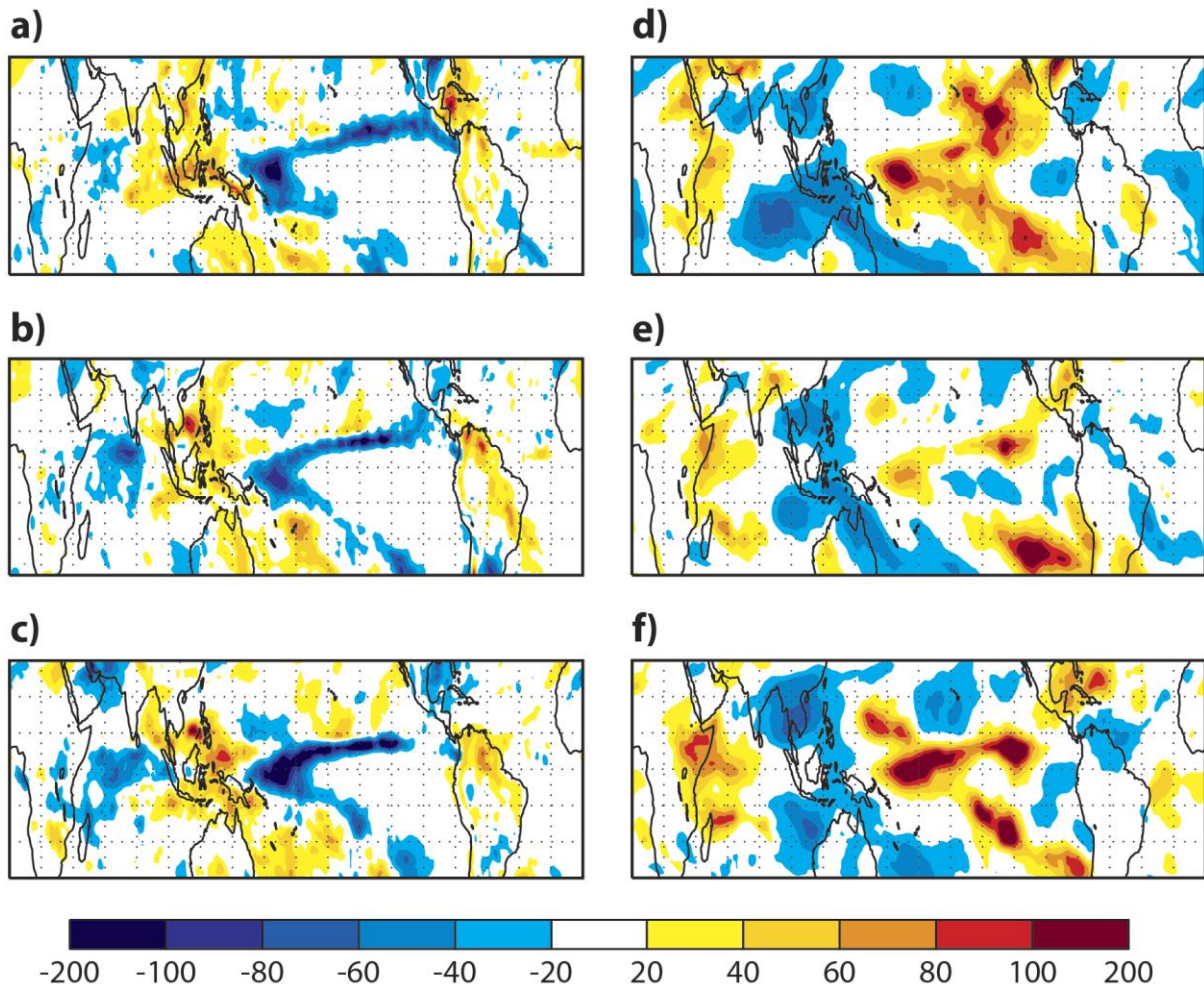
c)



1

1 Figure

2 2



3

4

5 Figure 2: Left panels: Anomaly of vertical velocity at 500 hPa in mm/s calculated from the

6 MACC reanalysis as the difference of El Niño composite minus La Niña composite for October

7 (a), November (b) and December (c). Blue colours show increased ascent, red colours increased

8 descent. Right panels: Specific humidity anomaly at 500 hPa in % calculated from the MACC

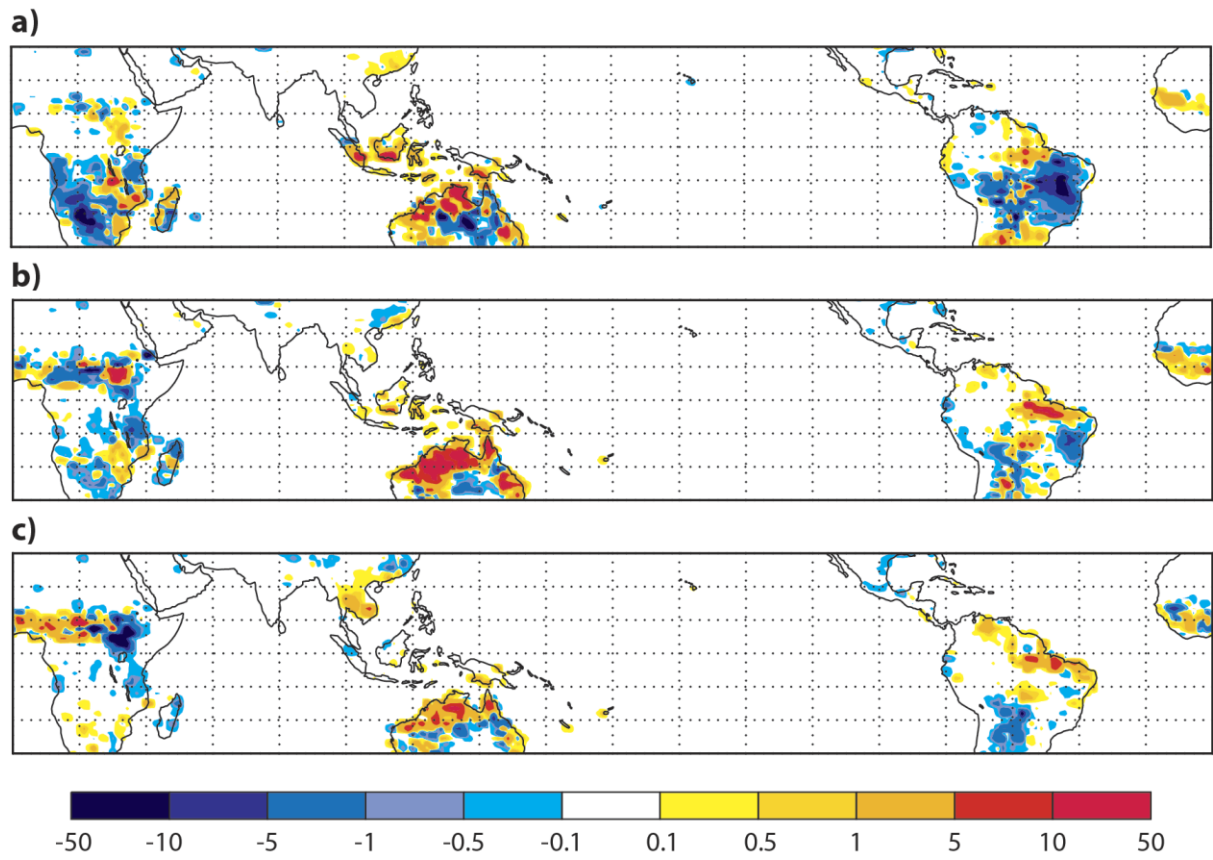
9 reanalysis as the difference of El Niño composite minus La Niña composite for October (d),

10 November (e) and December (f). Blue colours show reduced specific humidity, red colours

11 increased values.

12

1
2



3

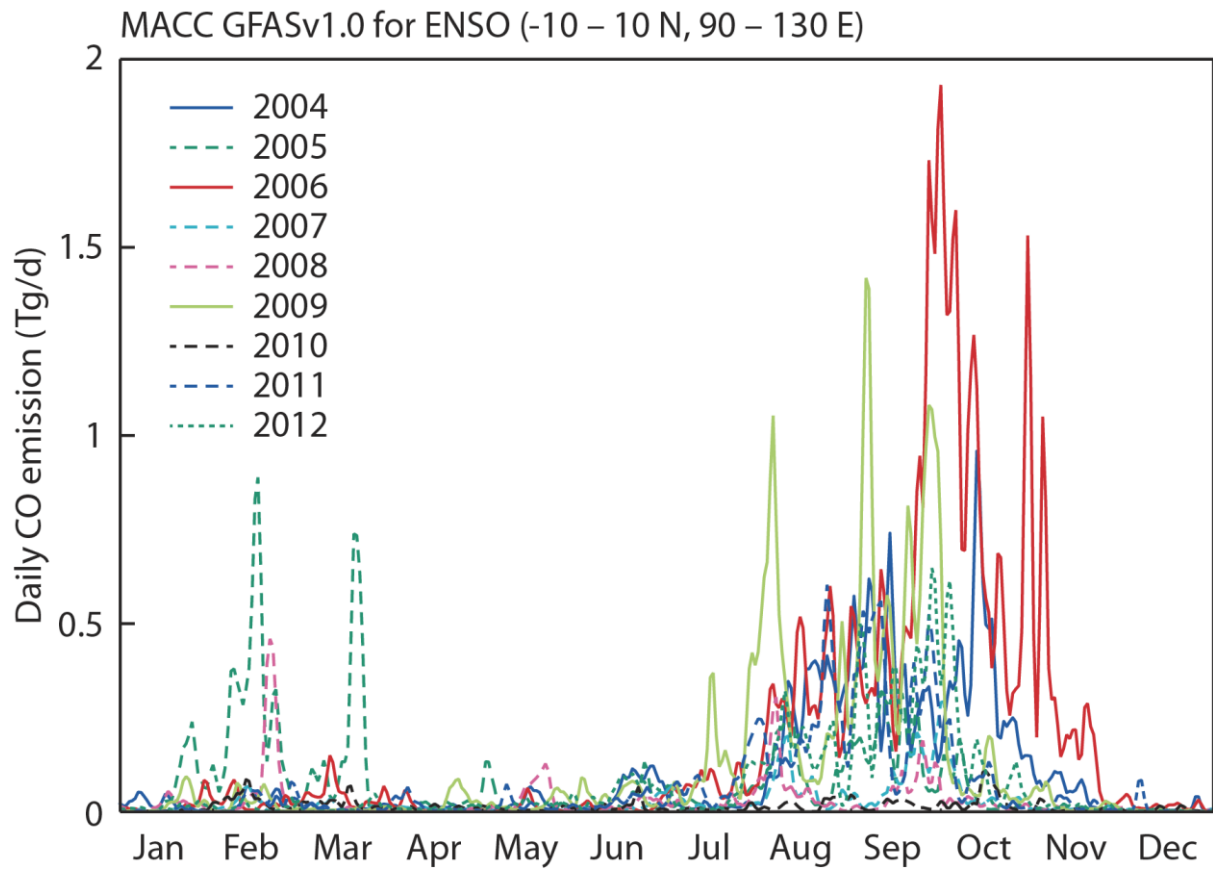
4

5

6

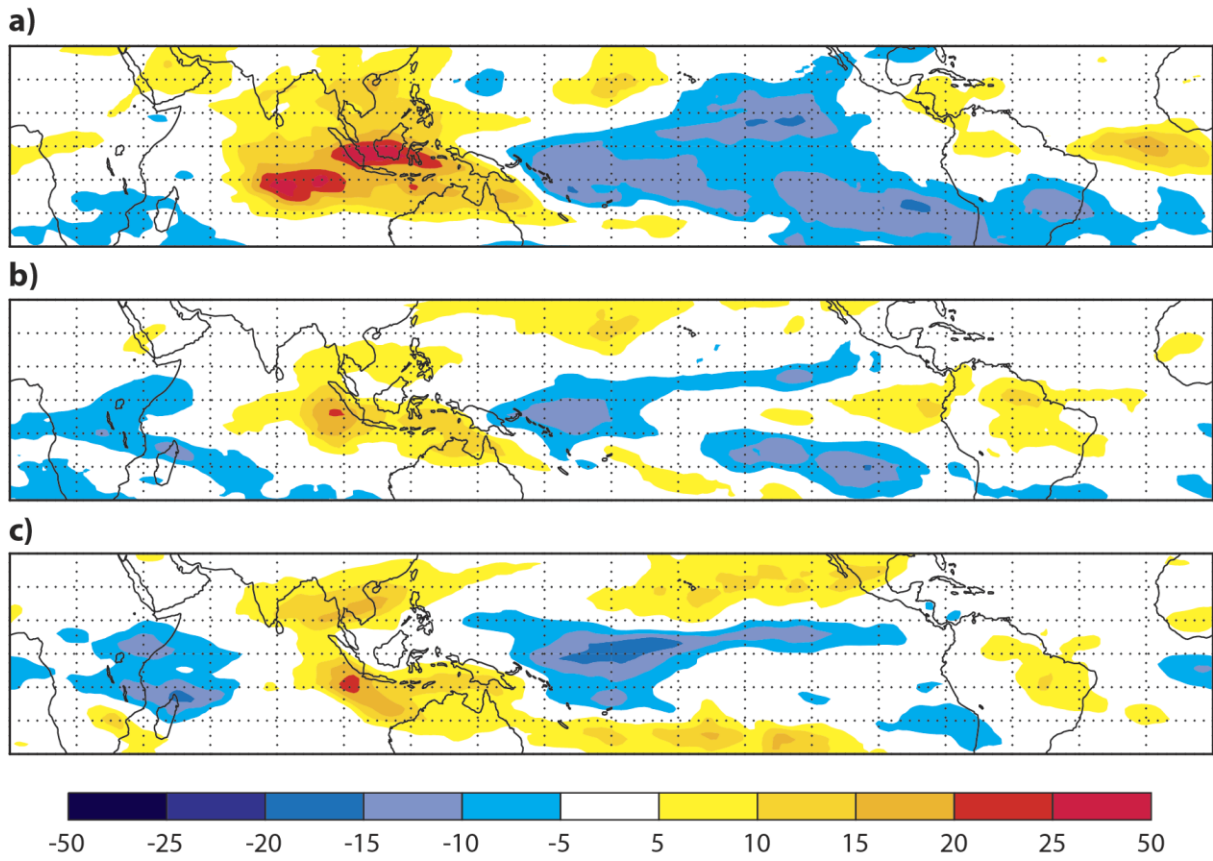
7

Figure 3: Biomass burning (fire radiative power areal density) anomaly in mW/m^2 calculated from the GFAS v1.0 dataset as the difference of El Niño composite minus La Niña composite for October (a), November (b) and December (c). Red colours indicate positive values, blue colours negative values.



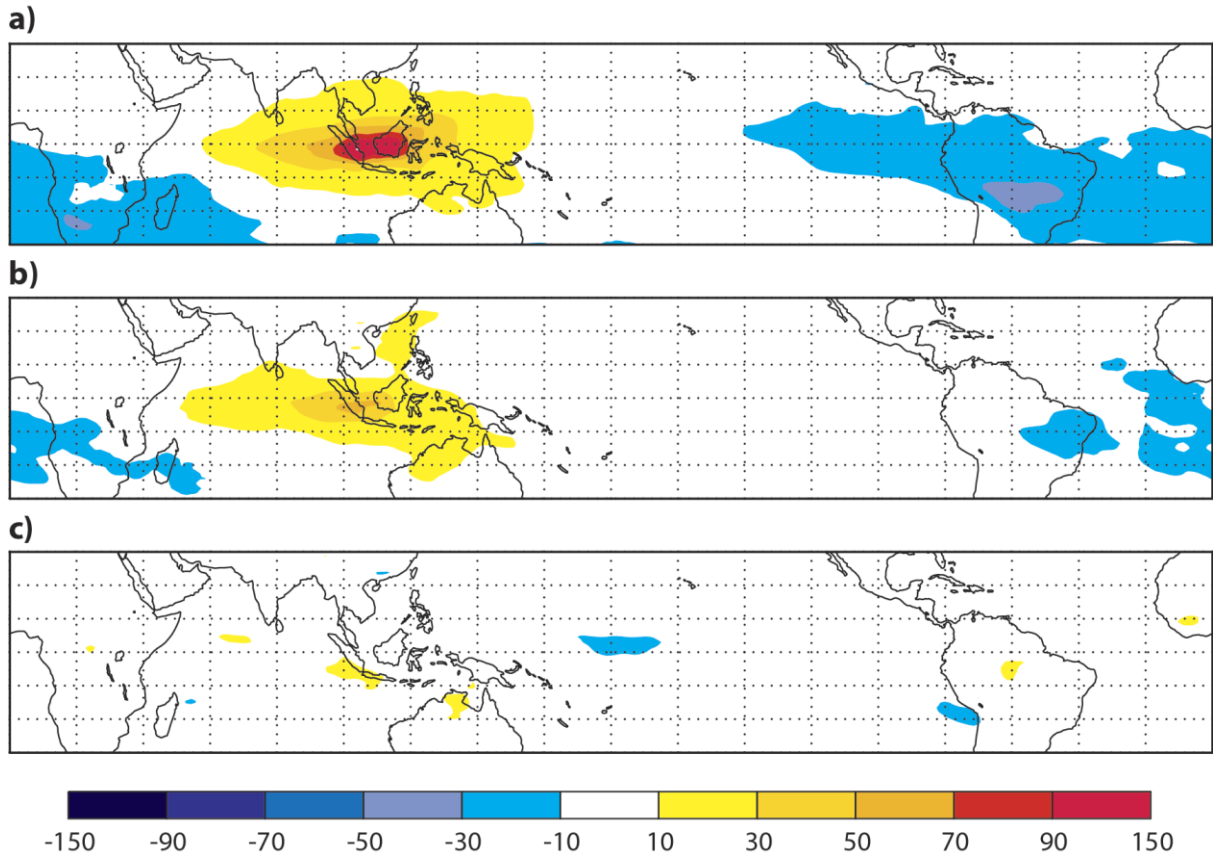
1
 2 Figure 34: Timeseries of daily CO emissions in Tg (10^{12} g) per day from GFASv1.0 for the
 3 region $10^{\circ}\text{N} - 10^{\circ}\text{S}$, $90^{\circ}\text{E} - 130^{\circ}\text{E}$ for the years 2003 to 2012.
 4

1



2

3 Figure 45: O₃ anomaly at 500 hPa in ppb calculated from the MACC reanalysis as the difference
4 of El Niño composite minus La Niña composite for October (a), November (b) and December
5 (c). Red colours indicate positive values, blue colours negative values.

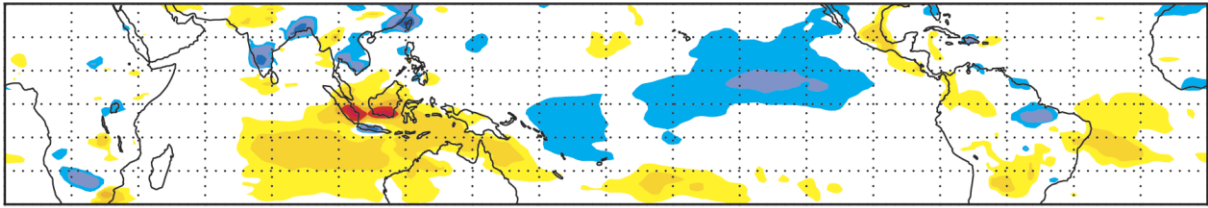


1
2
3

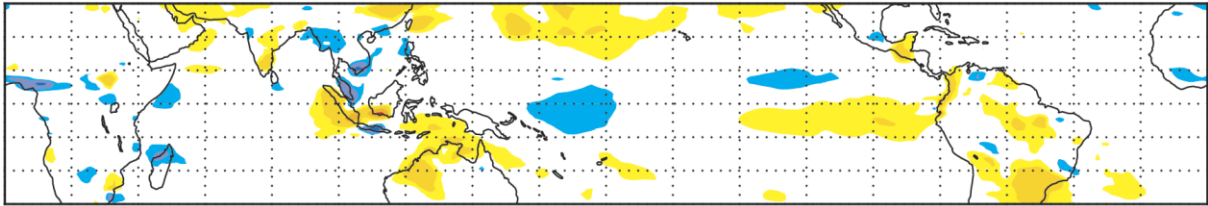
Figure 6: Like Figure 5: ~~Like Figure 4~~ but for CO anomaly at 500 hPa in ppb.

1

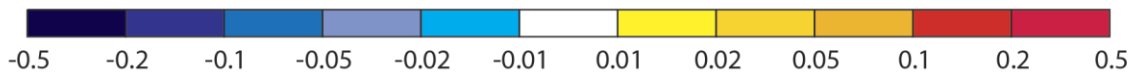
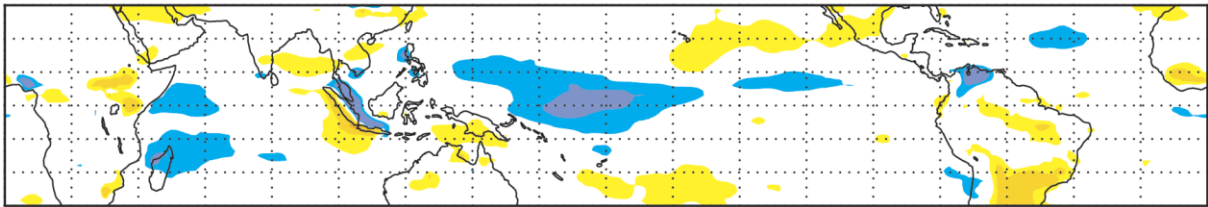
a)



b)



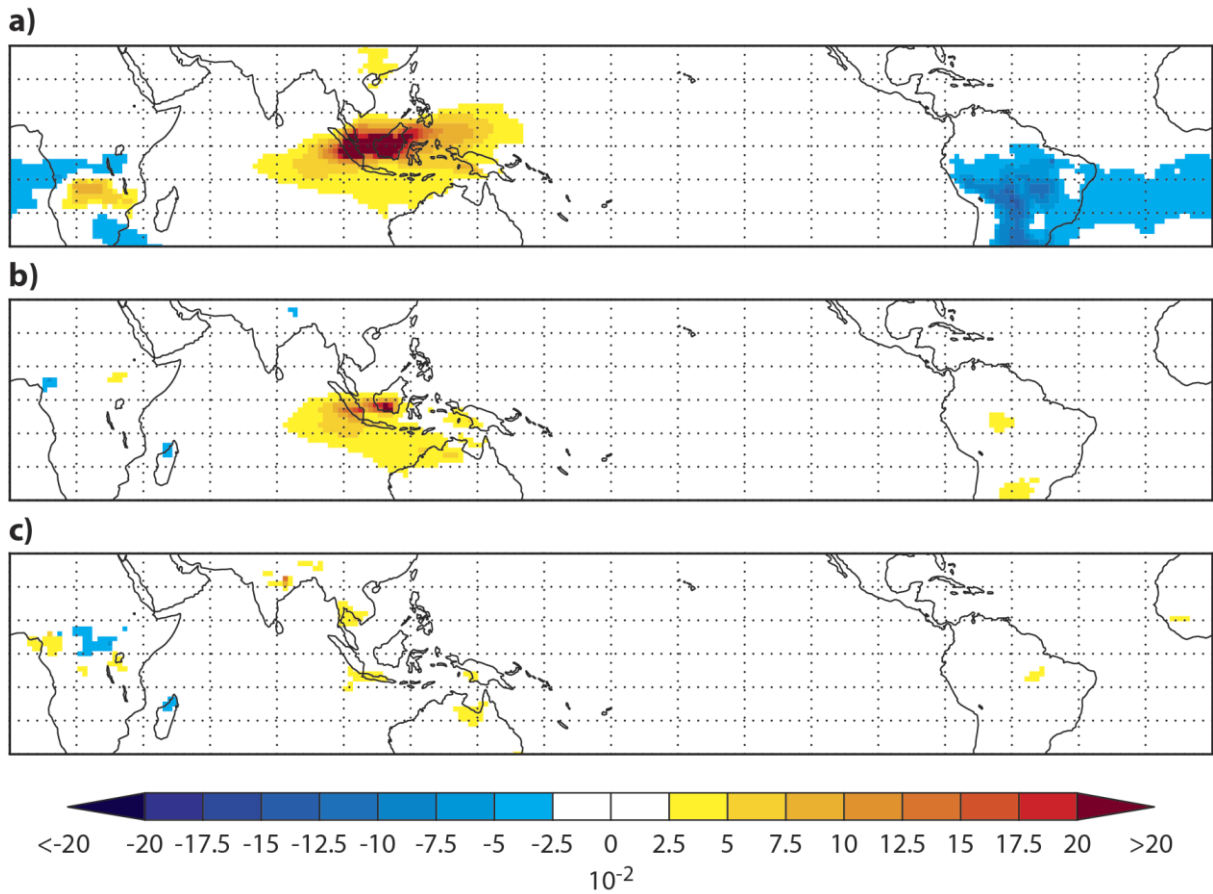
c)



2

3 Figure 67: Like Figure 45 but for NOx anomaly in ppb.

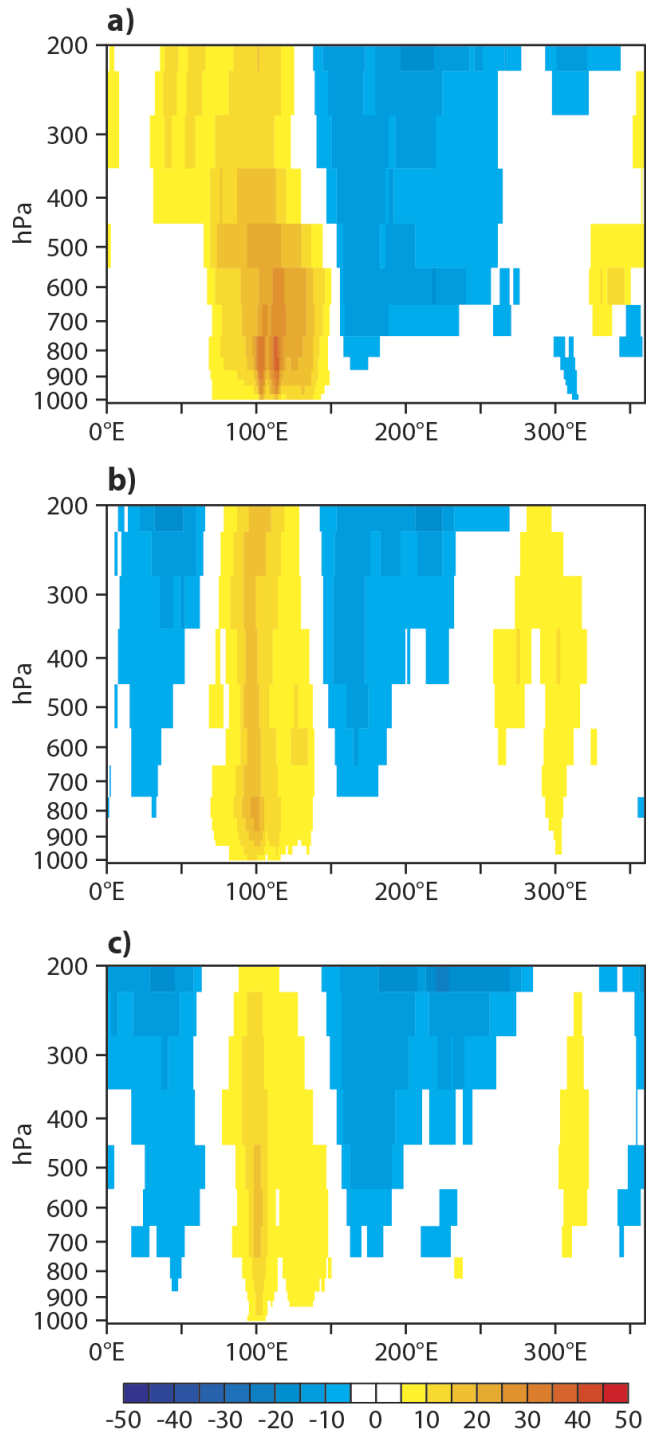
4



1

2 Figure 78: Like Figure 45 but for smoke AOD (BC+OM). AOD is unitless.

3

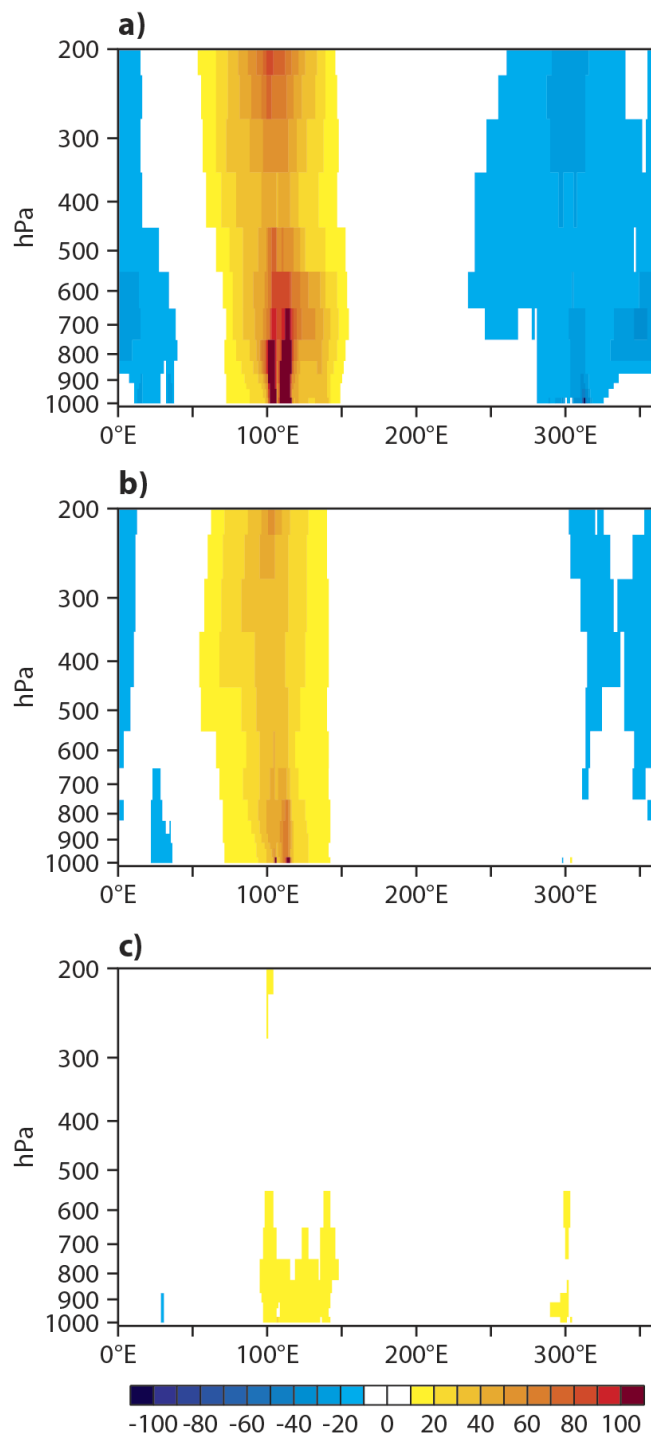


1

2 Figure 89: Vertical cross section of O₃ anomalies in ppb plotted against longitude and averaged
 3 between 0° and 12°S calculated from the MACC reanalysis as the difference of El Niño
 4 composite minus La Niña composite for October (a), November (b) and December (c). Red
 5 colours indicate positive values, blue colours negative values.

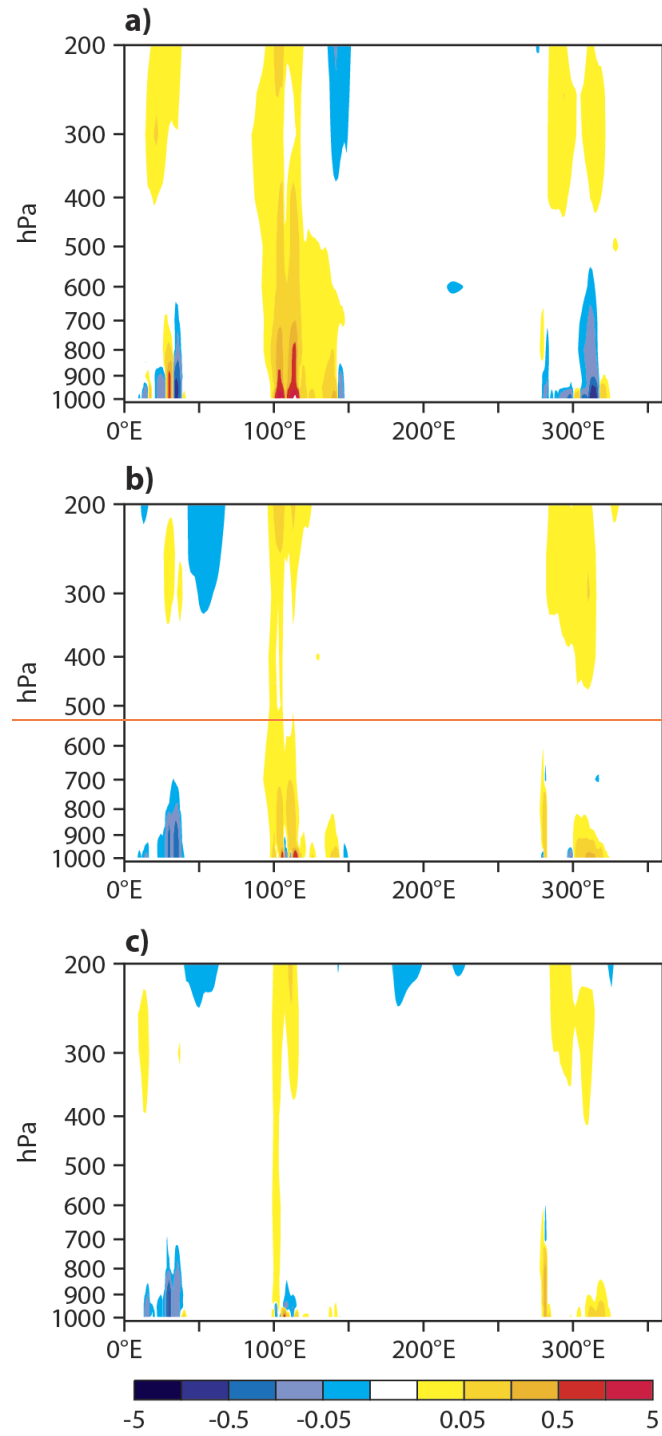
6

1



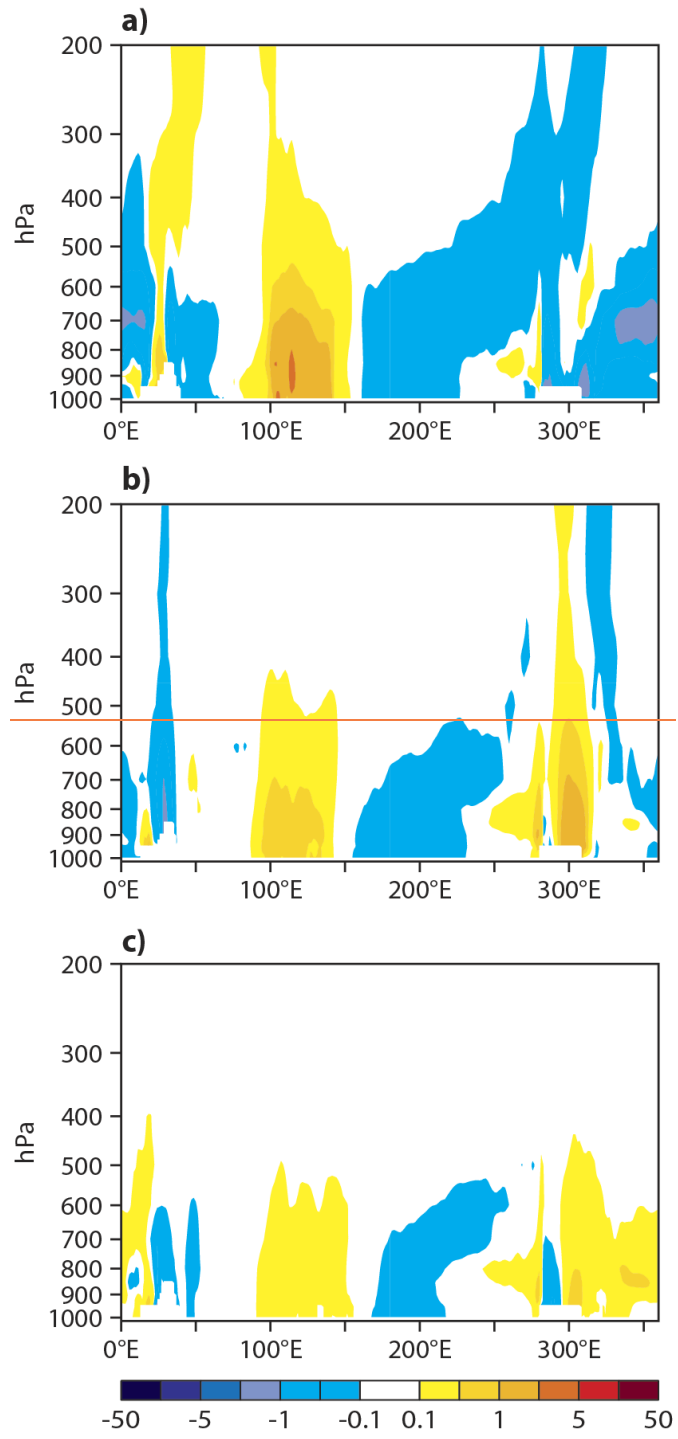
2

3 **Figure 9: Like Figure 8 but for CO in ppb.**

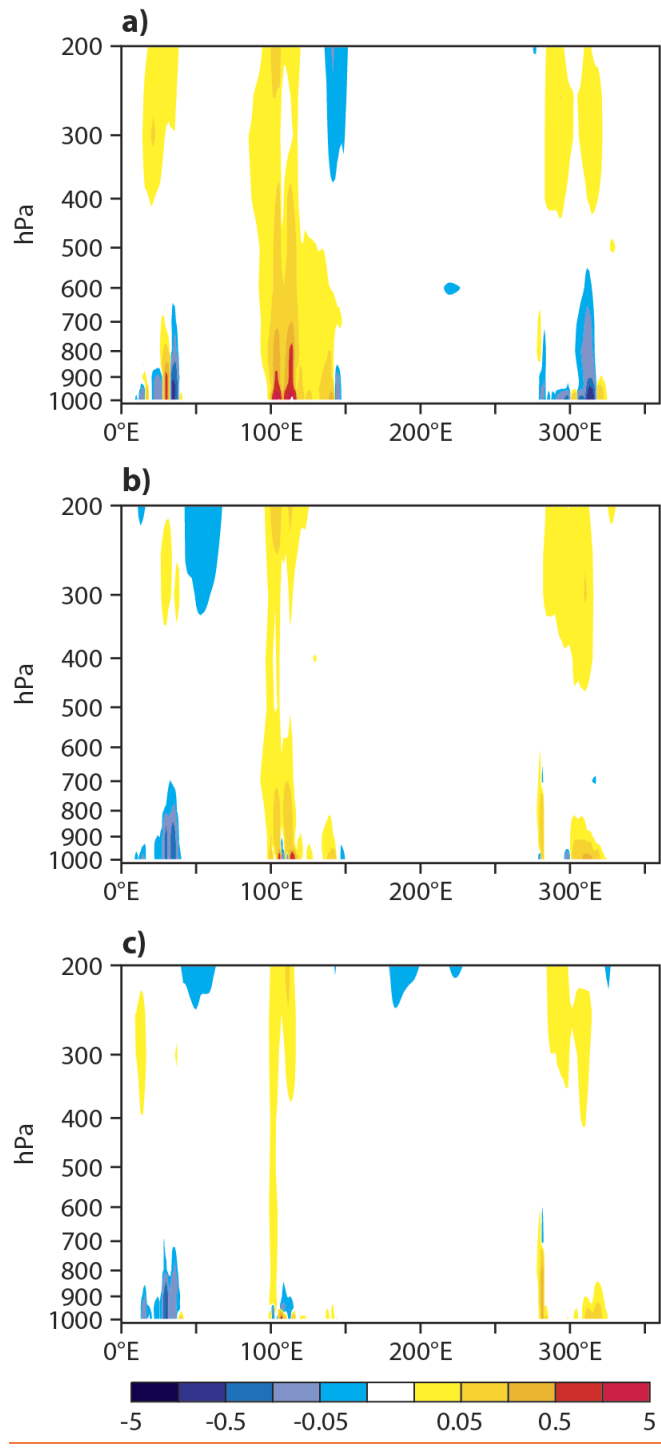


1

2 Figure 10: Like Figure 89 but for NO_x and CO in ppb.

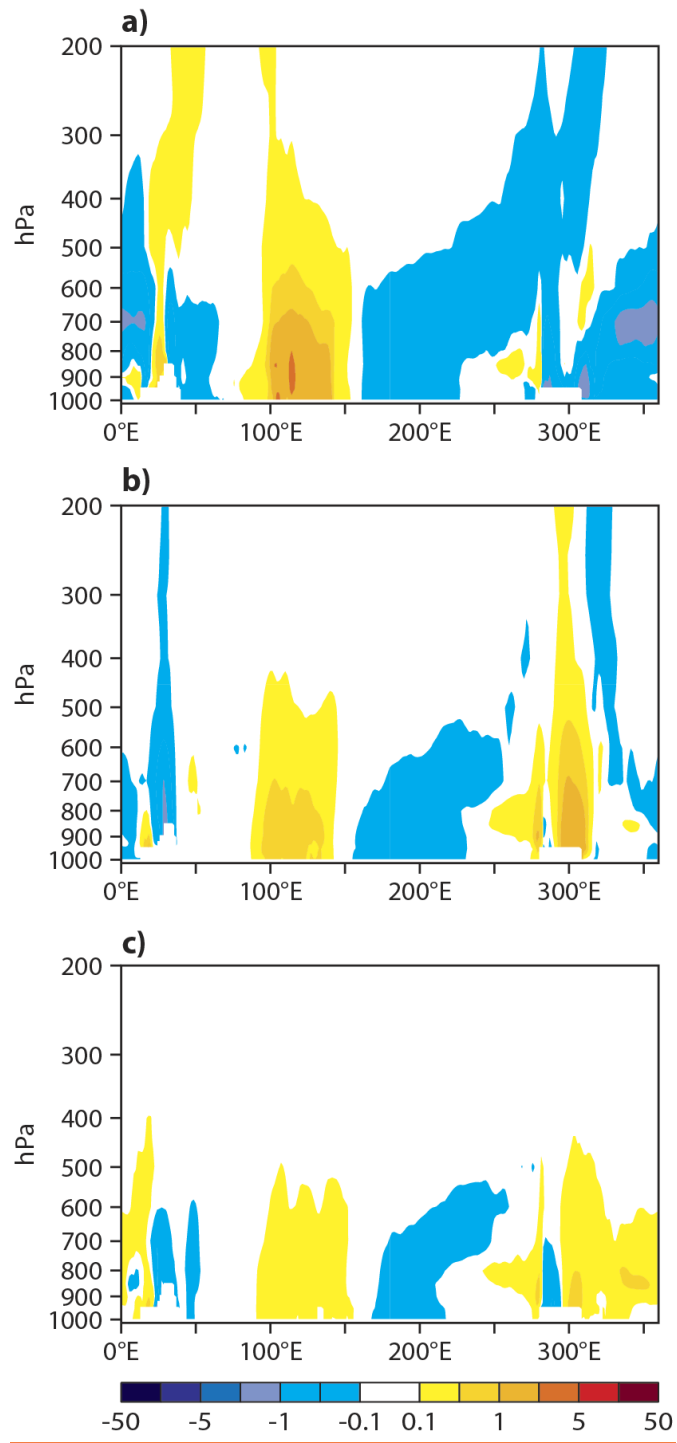


1



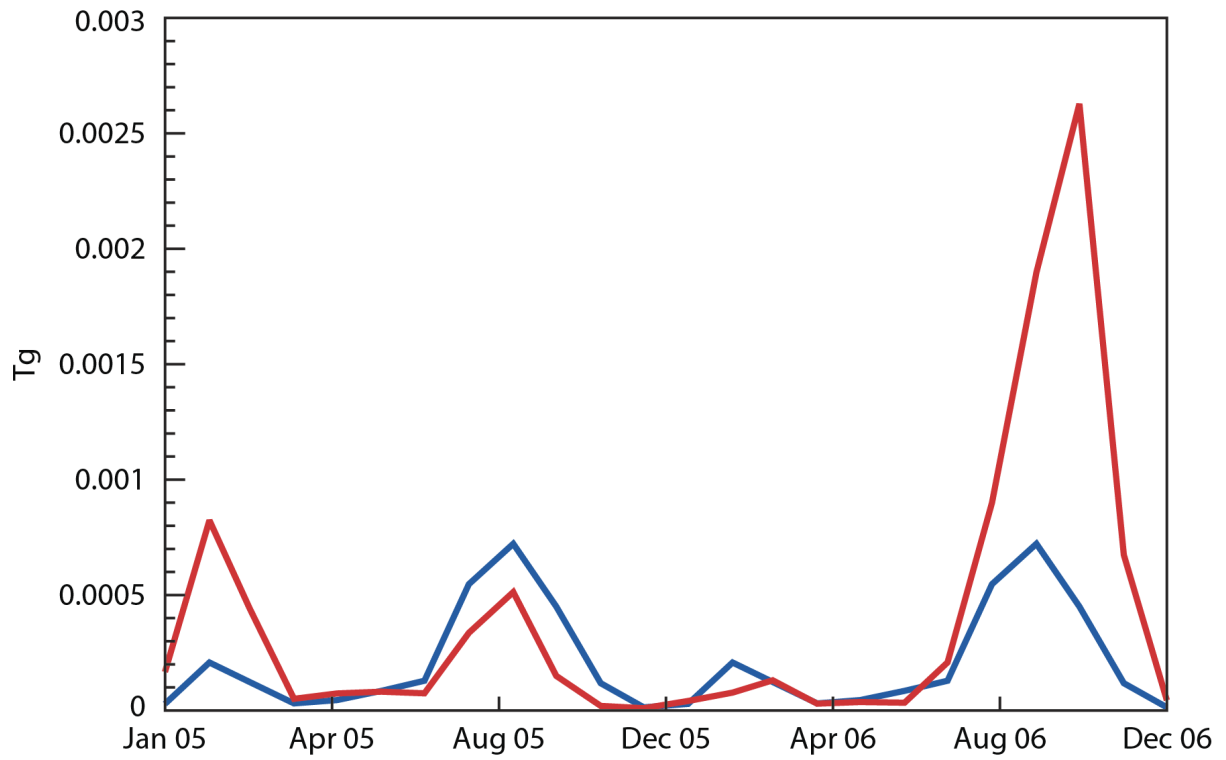
1

2 Figure 11: Like Figure 89 but for NOx in ppb.

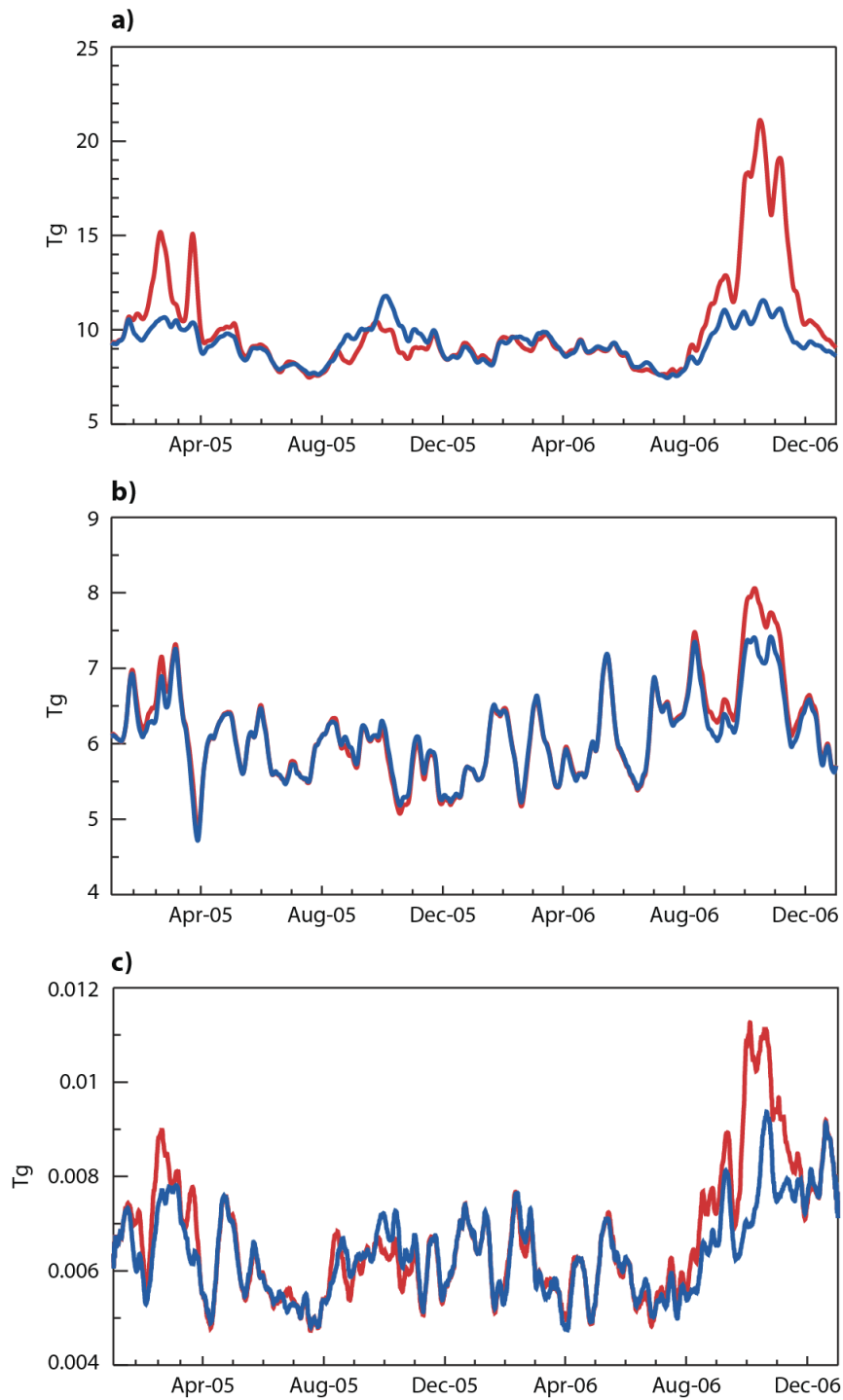


1

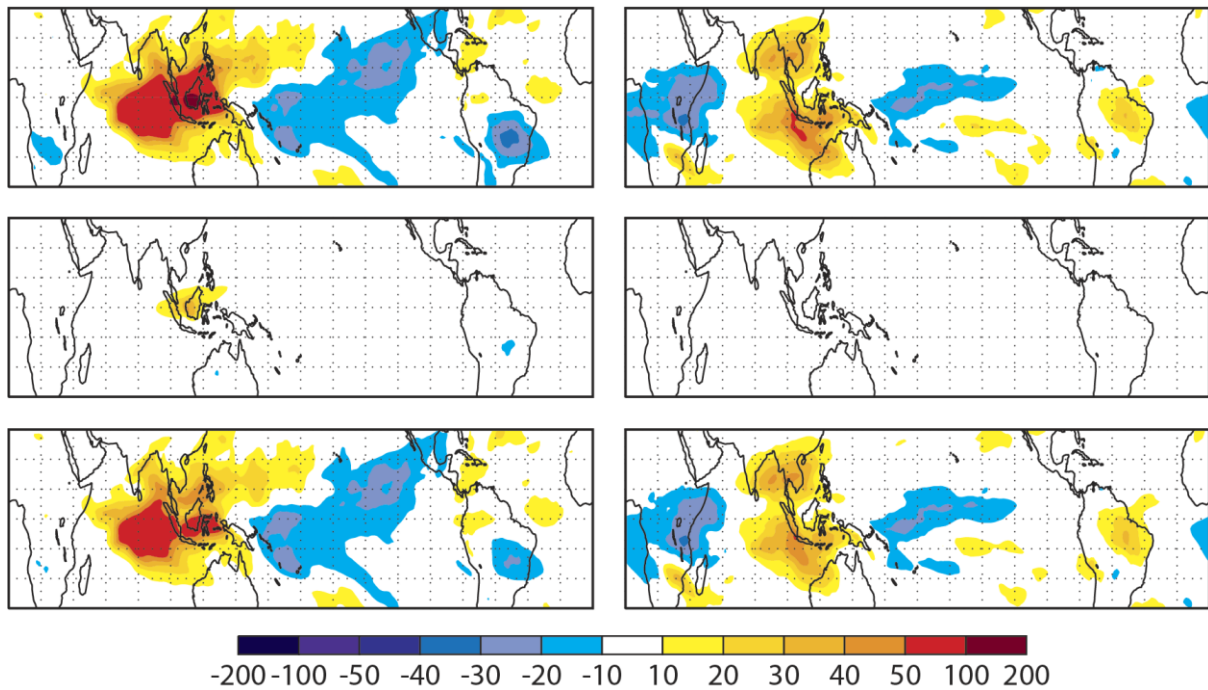
2 [Figure 12: Like Figure 9](#) but for smoke aerosol in ppb.



1
 2 Figure 4213: Timeseries of CO biomass burning emissions in Tg averaged over the region
 3 between 10°N, 10°S, 90°E, 130°E from GFAS v1.0 (red) and climatological GFAS v1.0 data set
 4 (blue.)



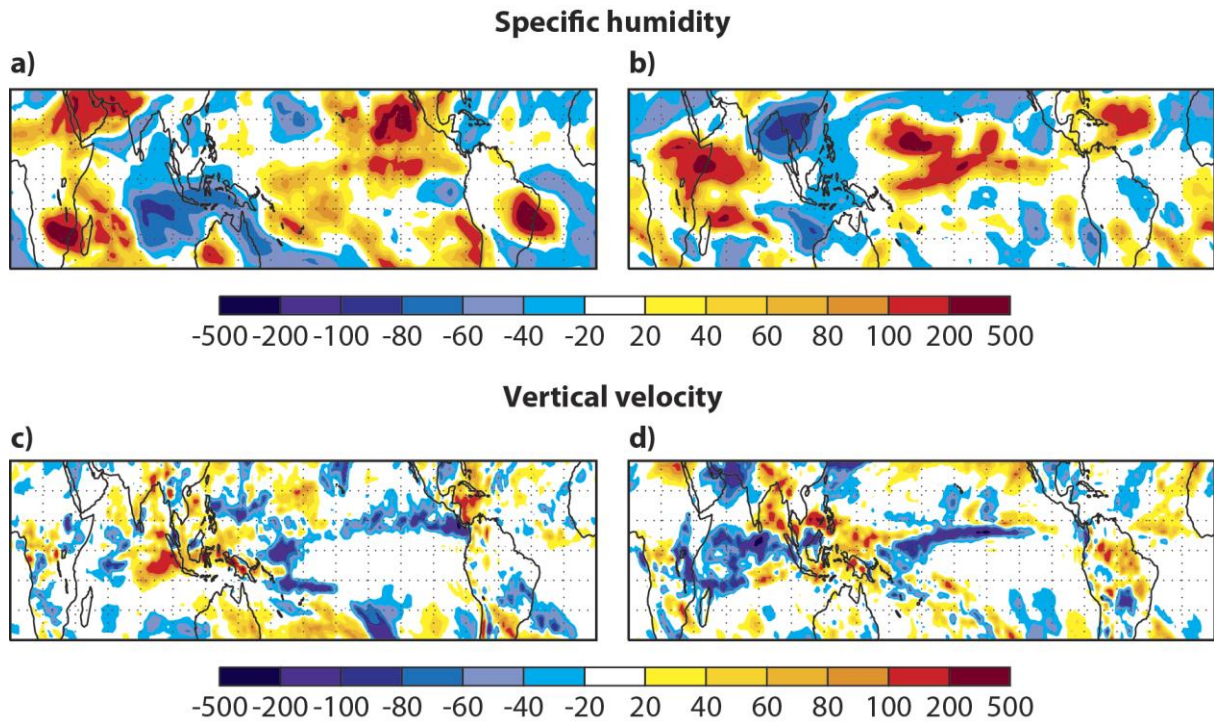
1
 2 Figure 1314: Timeseries of the tropospheric CO (a), O₃ (b), NO₂ (c) burden in Tg from BASE
 3 (red) and CLIM (blue) for 2005 and 2006 averaged over the area between 10°N, 10°S, 90°E,
 4 130°E.



1

2 Figure 14.15: TCO3 differences in % for October (left) and December (right) from the
 3 experiments BASE06 - BASE05 (top), BASE06 - CLIM06 (middle) and CLIM06 - CLIM05
 4 (bottom). The top panels show the overall differences of TCO3 due to the combined effects of
 5 El Niño related dynamical changes and changes in the fires emissions between El Niño and
 6 normal conditions. The middle panels show the impact of changes to the fire emissions under
 7 El Niño conditions, and the bottom panels show the impact of the El Niño induced dynamical
 8 changes on TCO3 when climatological fire emissions are used for both years. Red colours
 9 indicate positive values, blue colours negative values.

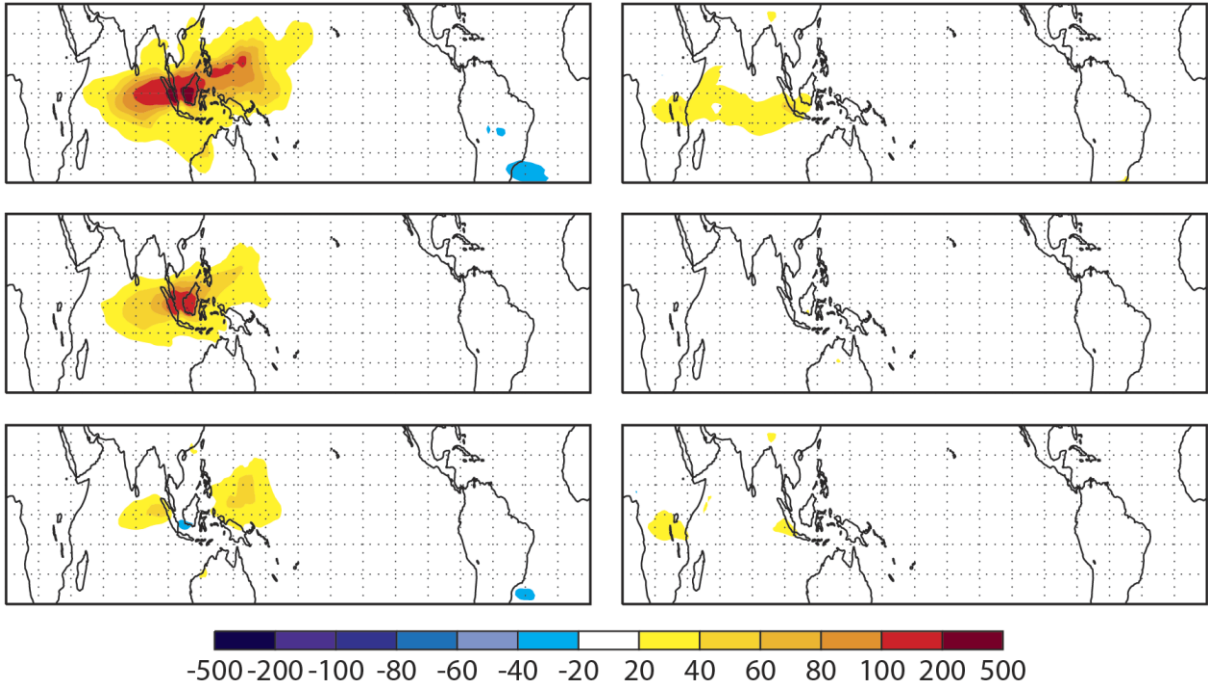
10



1
 2 Figure 4.516: Top panels: Specific humidity differences at 500 hPa in % for October (a) and
 3 December (b) from the experiments BASE06 minus BASE05. Blue colours show reduced
 4 specific humidity, red colours increased values. Bottom panels: Differences of vertical velocity
 5 in mm/s for October (c) and December (d) from the experiments BASE06 minus BASE05. Blue
 6 colours show increased ascent, red colours increased descent.

7

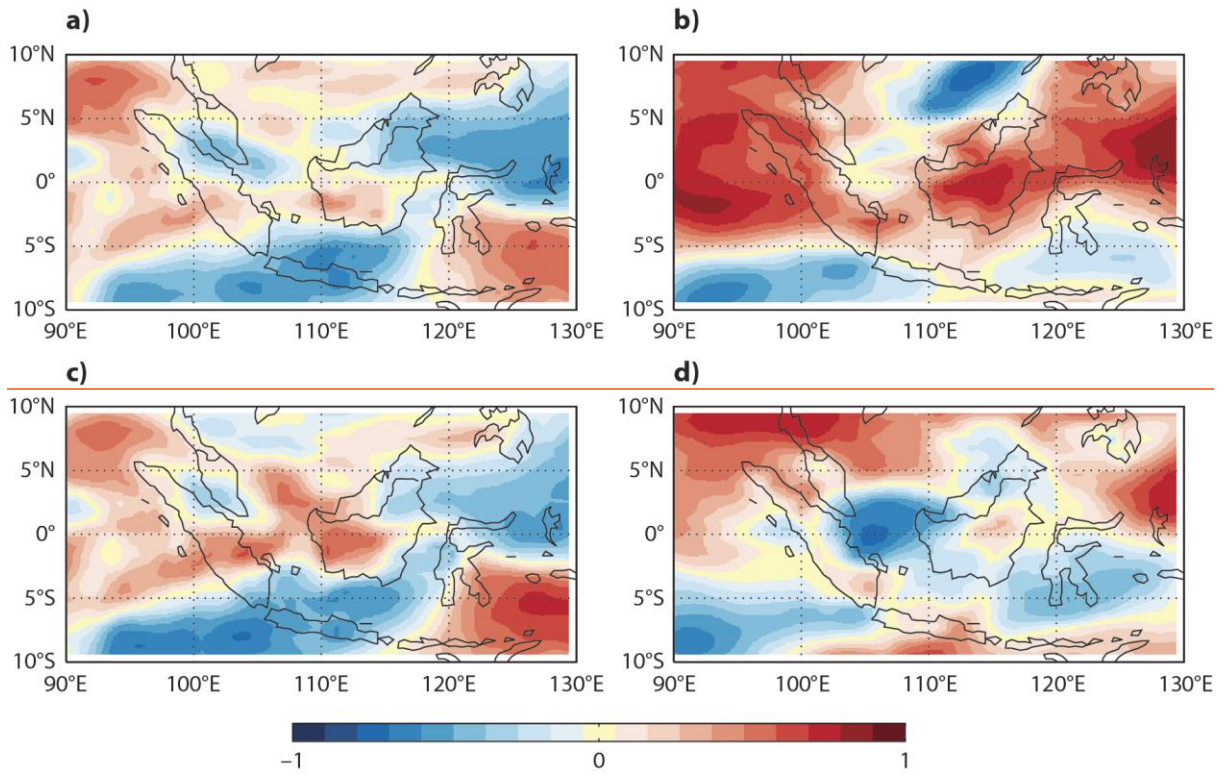
8



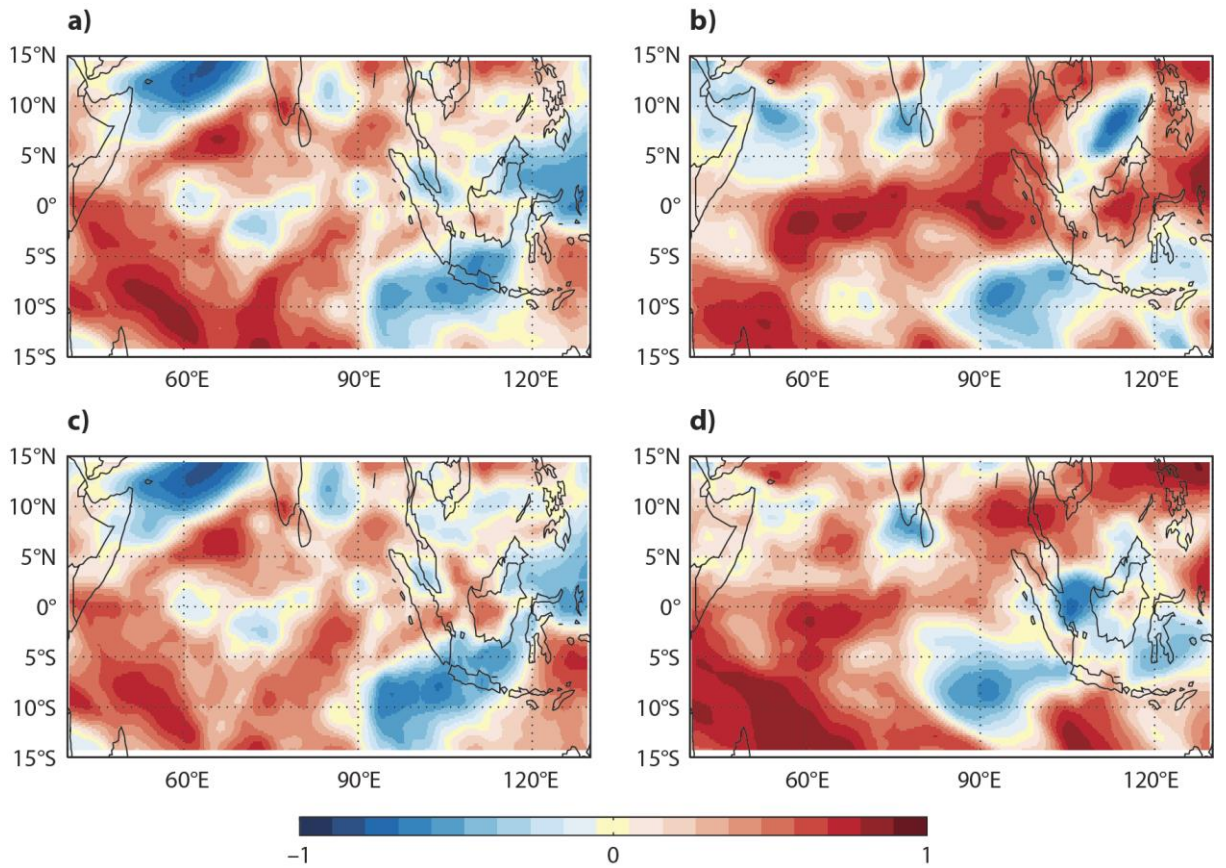
1

2 Figure 4617: TCCO differences in % for October (left) and December (right) from the
 3 experiments BASE06 - BASE05 (top), BASE06 - CLIM06 (middle) and CLIM06 - CLIM05
 4 (bottom). Red colours indicate positive values, blue colours negative values.
 5

1



2



3

1 Figure 4718: October O₃-CO correlations calculated for free tropospheric (approx. 750-350
2 hPa) column abundances over the Maritime Continent from the BASE (top) and CLIM (bottom)
3 experiments for 2005 (left) and 2006 (right). Red colours indicated positive correlations, blue
4 colours negative ones.

5